Water Resources Research

RESEARCH ARTICLE
10.1029/2021WR031017

An Interactively Corrected Smoothed Particle Hydrodynamics (IC-SPH) for Simulating Solute Transport in a Nonuniform Velocity Field

Tian Jiao[1,2,3], Ming Ye[2,3], Menggui Jin[1], and Jing Yang[1,2,3]

[1]School of Environmental Studies, China University of Geosciences, Wuhan, China, [2]Department of Earth, Ocean, and Atmosphere Science, Florida State University, Tallahassee, FL, USA, [3]Department of Scientific Computing, Florida State University, Tallahassee, FL, USA

Abstract The Smoothed Particle Hydrodynamics (SPH) method is a Lagrangian approach that has been widely used to eliminate numerical dispersion for solving advection-dispersion equation (ADE) of groundwater solute transport under advection-dominated situations. It has been found that accuracy of SPH results is severely deteriorated, when particles are irregularly distributed in a model domain with heterogeneous hydraulic conductivity. To resolve this problem, we developed a new approach called Interactively Corrected SPH (IC-SPH), which is an improved version of the Corrected SPH (C-SPH) method. IC-SPH uses an interactively corrected kernel gradient to construct concentration gradients used to solve ADE. This correction is made for each particle by using not only the particle's neighbor particles within the particle's support domain but also the particles within each neighbor particle's support domain. We evaluated IC-SPH performance in two numerical studies. One considers diffusive transport with an analytical solution, and the other considers advection-dispersion transport in a heterogeneous field of hydraulic conductivity. For each numerical study, several numerical experiments were conducted using multiple sets of irregularly distributed particles with different levels of particle irregularity. The numerical experiments indicate that, while IC-SPH is more computationally expensive than SPH and C-SPH, IC-SPH produces more accurate ADE solutions, and converges faster to the analytical solution. IC-SPH is mathematically general, and can be applied to a wide range of problems that require solving ADE.

Key Points:

- Interactively Corrected Smoothed Particle Hydrodynamics (IC-SPH) is developed as a new method for groundwater solute transport modeling
- Kernel gradients are corrected by using not only neighbor particle *j* of particle *i* but also particles in the support domain of each particle *j*
- IC-SPH outperforms SPH and a corrected SPH methods when solving advection-dispersion equations for irregularly distributed particles

Supporting Information:

Supporting Information may be found in the online version of this article.

Correspondence to:

M. Ye and M. Jin,
mye@fsu.edu;
mgjin@cug.edu.cn

Citation:

Jiao, T., Ye, M., Jin, M., & Yang, J. (2022). An Interactively Corrected Smoothed Particle Hydrodynamics (IC-SPH) for simulating solute transport in a nonuniform velocity field. *Water Resources Research*, *58*, e2021WR031017. https://doi.org/10.1029/2021WR031017

Received 9 AUG 2021
Accepted 9 MAY 2022

Author Contributions:

Conceptualization: Ming Ye, Menggui Jin
Formal analysis: Tian Jiao
Methodology: Tian Jiao, Ming Ye, Menggui Jin
Software: Jing Yang
Supervision: Ming Ye, Menggui Jin
Writing – original draft: Tian Jiao
Writing – review & editing: Ming Ye, Menggui Jin, Jing Yang

1. Introduction

When numerically solving advection-dominated solute transport problems using Lagrangian approaches, Smoothed Particle Hydrodynamics (SPH) methods have been found to often perform better than traditional Eulerian schemes for solving the advection-dispersion equation (ADE) due to SPH's ability of eliminating numerical dispersion (Benson & Meerschaert, 2008; Benson et al., 2017; Bolster et al., 2016; Boso et al., 2013; de Barros et al., 2015; Herrera et al., 2009, 2017; Sole-Mari & Fernàndez-Garcia, 2018; Sole-Mari et al., 2017, 2019; Tartakovsky et al., 2007a, 2007b, 2009, 2015). Boso et al. (2013) compared SPH with four mesh-based and Lagrangian methods for simulating nonreactive and reactive solute transport in heterogeneous porous media, and showed the potential of SPH to reduce the impacts of numerical dispersion on numerical ADE solutions. However, SPH is subject to numerical errors, and the integral interpolation schemes used in SPH are subject to two errors: smoothing errors and numerical discretizing errors (Monaghan, 2005; Zhu et al., 2015). The smoothing error is caused by the integral interpolation, and it depends on the shape and smoothing length of the kernel functions used in SPH. The numerical discretizing error is caused by the summation of discrete particles in the integral, and it depends on the particle number and particle distribution within a support domain associated with the integral (Herrera et al., 2009; Liu & Liu, 2010; Monaghan, 2005; Zhu et al., 2015). For a kernel function with a fixed smoothing length, accuracy of SPH solutions depends on the number and spatial distribution of the particles located in the support domain (Liu & Liu, 2010; Monaghan, 2005). Previous studies showed that SPH performs well for evenly spaced particles in a modeling domain (Herrera et al., 2009; Liu & Liu, 2010; Monaghan, 2005). When evenly spaced particle distribution cannot be maintained, accuracy of SPH solutions decreases. Particle irregularity occurs commonly in heterogeneous porous media with nonuniform velocity fields (in terms of both velocity direction and magnitude), due to particles moving with flow. This is a prevalent problem, since real-world aquifers are heterogeneous in nature (Bellin et al., 1993; Konikow, 2011). Previous studies

of groundwater solute transport modeling have shown that accuracy of SPH methods decreases in heterogeneous aquifers (Avesani et al., 2015; Herrera & Beckie, 2013; Herrera et al., 2009; Tartakovsky, 2010).

There have been several studies that improve particle approximation accuracy of SPH for irregularly districted particles. Avesani et al. (2015) developed a modified SPH method based on the Moving-Least-Squares-Weighted-Essentially-Non-Oscillatory (MLS-WENO) reconstruction of concentrations. The method applies MLS-WENO to moving particles for accurate reproduction of concentration and concentration gradients, and is less sensitive to particle spatial distributions due to an improved estimation of spatially varying concentration fluxes. However, this method is computationally expensive due to intermediate steps involved in MLS-WENO reconstruction of concentration gradients. When using comparable particle spacings and support domains, the modified SPH method requires up to 2 orders of magnitude more CPU time than SPH does. Although the computational time of the modified SPH can be reduced by using the ADER-WENO-SPH method (ADER standing for Arbitrary DERivatives) developed by Avesani et al. (2021) or an SPH scheme based on Moving-Least Squares reconstructions in combination with a posteriori Multidimensional Optimal Order Detection (MOOD; Clain et al., 2011; Nogueira et al., 2016), these methods have not been applied to groundwater solute transport problems. Alvarado-Rodríguez et al. (2019) improved the accuracy of SPH for irregularly distributed particles by adjusting the number of neighbor particles in a support domain based on the relation between the support domain size and the number of particles; the relation was derived by Sigalotti et al. (2016) and Zhu et al. (2015). Using a large number of neighbor particles requires a large amount of computational memory. In addition, adjusting the number of neighbor particles is not straightforward because the degree of particle irregularity changes in space and time.

Efforts have been spent to improve SPH with irregular particle distributions in the field of groundwater modeling and other fields. Since accuracy of SPH solutions partly depends on discretizing error (i.e., the number of particles in a support domain), a straightforward method to improve SPH accuracy is to increase the number of neighbor particles (Sigalotti et al., 2016; Zhu et al., 2015). This approach is practically difficult due to the demands of high computational cost and memory. Another way to improve SPH accuracy is to correct the SPH kernel function and/or its derivatives by using a Taylor series expansion method (e.g., Chen & Beraum, 2000; Liu et al., 2005; Zhang & Batra, 2004). For example, Chen and Beraum (2000) and Chen et al. (1999) developed a Corrected Smoothed Particle Hydrodynamics (C-SPH) which improves simulation accuracy inside a model domain and around the domain boundaries. Following Chen and Beraum (2000), Liu et al. (2005) developed a finite particle method, which uses a set of basis function to approximate variables of interest and their derivatives at a set of arbitrarily distributed particles (Liu & Liu, 2006; Liu et al., 2005), and then this method is coupled with particle shifting technique to model particulate flows with thermal convection (Zhang et al., 2019). Based on an idea similar to that of the finite particle method, Zhang and Batra (2004) concurrently developed a modified SPH method for studies of solid mechanics (Batra & Zhang, 2004; Zhang & Batra, 2008). The core idea behind these methods is similar to that in C-SPH. C-SPH uses a Taylor series expansion to correct kernel gradients for improving particle approximation accuracy, and is less sensitive to particle irregularity.

The C-SPH method can be further improved, because the C-SPH correction for kernel gradients only considers neighbor particles within the support domain of a particle of interest (say particle i). Considering that a kernel function and its gradient are determined jointly by particle i and its neighbor particles j, we hypothesized that, if we correct the kernel gradient with neighbor particles within the support domains of particle i and particle j, then accuracy of C-SPH can be improved. Based on this idea, we develop a new method called Interactively Corrected Smoothed Particle Hydrodynamics (IC-SPH), and apply it to solve ADE for simulating solute transport in heterogeneous aquifers.

IC-SPH uses an interactively corrected matrix generated by using a Taylor series expansion to correct kernel gradients. While it is common to use Taylor series expansion for improving SPH (Batra & Zhang, 2004; Chen & Beraum, 2000; Chen et al., 1999; Liu et al., 2005; Xu & Deng, 2016; Zhang & Batra, 2004, 2008), our IC-SPH method is different from other modified SPH methods, in that IC-SPH considers the particles in the support domain of a particle of interest and its neighbor particles. We show in two numerical experiments that IC-SPH outperforms SPH and C-SPH when the level of particle irregularity increases. The first experiment considers only diffusive transport, and has an analytical solution that can be used to evaluate accuracy of SPH, C-SPH, and IC-SPH solutions. The second experiment considers both advection and dispersion in a domain with heterogeneous hydraulic conductivity, and uses a numerical solution as a reference to evaluate accuracy of IC-SPH solution.

2. Mathematical Model and Numerical Schemes

The ADE in porous media with the Lagrangian coordinates is described as

$$\frac{d\mathbf{x}}{dt} = \mathbf{v} \tag{1}$$

$$\frac{dC}{dt} = \nabla \cdot (\mathbf{D}\nabla C) \tag{2}$$

where C is the solute concentration, $\mathbf{D}$ is the local-scale dispersion coefficient defined by Bear (1972), $\mathbf{v}$ is a vector of seepage velocity, and $\mathbf{x}$ is the position of a fluid particle. The substantial derivative, $dC/dt = \partial C/\partial t + \mathbf{v}\partial C/\partial \mathbf{x}$, represents time rate change of solute concentration along the pathline of a particle. In a component form, advection and dispersion terms are presented by Equations 1 and 2, respectively.

2.1. SPH Discretization of the Dispersion Term

In an SPH scheme, Equations 1 and 2 are approximated by using a finite number of particles to carry the solute concentration. Equation 1 governs the particle movement, and the solution of Equation 2 is evaluated by using a kernel interpolation approximation. Kernel interpolation approximation of concentration $C(\mathbf{x}_i, t)$ and its first-order derivative $\nabla C(\mathbf{x}_i, t)$ in space of the particle located at the position $\mathbf{x}_i$ at time t is approximated through the following Monte Carlo integration scheme (Boso et al., 2013; Herrera et al., 2009; Monaghan, 2005)

$$\langle C(\mathbf{x}_i, t)\rangle = \sum_{j=1}^{N_b} \frac{1}{n_j} C(\mathbf{x}_j, t)\, W_{ij}(\mathbf{x}_i - \mathbf{x}_j, h) \tag{3}$$

$$\langle \nabla C(\mathbf{x}_i, t)\rangle = \sum_{j=1}^{N_b} \frac{1}{n_j} (C(\mathbf{x}_j, t) - C(\mathbf{x}_i, t))\, \nabla_i W_{ij}(\mathbf{x}_i - \mathbf{x}_j, h) \tag{4}$$

where W is a kernel function, N_b is the number of neighbor particles within support domain the ith particle and the support domain is controlled by smoothing length h, particle number density, $n_j = \rho_j/m_j = 1/V_j$, is expressed as $n_j = \sum_k W(\mathbf{x}_j - \mathbf{x}_k, h)$ (Tartakovsky & Meakin, 2005), i.e., the number of particles per unit volume, where $\mathbf{x}_k$ is the location of neighbor particles of particle j.

More details of the SPH methods related to this study are given in Appendix A, which also explains impacts of particle irregularity on accuracy of SPH solutions by using a cubic B-spline function as an example kernel function. Based on the SPH solution of the heat-conduction equation by Cleary and Monaghan (1999), Espanol and Revenga (2003) derived the SPH integral approximation of dispersive fluxes. According to Alvarado-Rodríguez et al. (2019) and Herrera et al. (2009), the SPH approximation of Equation 2 for particle i is given as

$$\frac{dC_i}{dt} = \frac{1}{2} \sum_{j=1} \frac{1}{n_{ij}} (C_i - C_j)\, D_{ij} \frac{\mathbf{x}_i - \mathbf{x}_j}{|\mathbf{x}_i - \mathbf{x}_j|^2} \cdot \nabla_i W_{ij} \tag{5}$$

where $C_i = C(\mathbf{x}_i)$ and $C_j = C(\mathbf{x}_j)$ are the concentrations of the ith and jth particles, respectively, $n_{ij} = 2n_i n_j/(n_i + n_j)$ is the harmonic mean of n_i and n_j that are particle density number at position $\mathbf{x}_i$ and $\mathbf{x}_j$. D_{ij} is set as $D_{ij} = 2\left(D^i + D^j\right)$ for isotropic dispersion problem and $D_{ij} = \sum_\alpha \sum_\beta \left(D^i_{\alpha\beta} + D^j_{\alpha\beta}\right)\left(\Gamma(\mathbf{x}_i - \mathbf{x}_j)_\alpha (\mathbf{x}_i - \mathbf{x}_j)_\beta / |\mathbf{x}_i - \mathbf{x}_j|^2 - \delta_{\alpha\beta}\right)$ for anisotropic dispersion problem, $\Gamma = 4$ and 5 in a two-dimensional and three-dimensional space, respectively (Espanol & Revenga, 2003; Yildiz et al., 2009), α and β are the dimension indices ranging from 1 to 3 (i.e., from x to z), $D^i_{\alpha\beta}$ is a component of the dispersion coefficient tensor related to particle i, and $\delta_{\alpha\beta}$ is the Kronecker delta function. This study is mainly focused on isotropic dispersion problems. The derivation of Equation 5 for isotropic problems is given in Jubelgas et al. (2004) and Herrera et al. (2009), and the derivation for anisotropic problems is given in Espanol and Revenga. (2003), Yildiz et al. (2009), and Alvarado-Rodríguez et al. (2019). It is noted that Equation 5 uses a hybrid expression of SPH first-order derivative and a finite difference approximation of the first-order derivative. The second-order derivative in the dispersion term of Equation 2 is evaluated by using the first-order derivative of kernel. Morris et al. (1997) and Monaghan (2005) pointed out that this evaluation is less sensitive to particle irregularity, in comparison with the evaluation that employs the second-order derivative

of smoothing kernel function to directly approximate the concentration in Equation 3 (Herrera et al., 2009; Monaghan, 2005; Morris et al., 1997). This is further explained in Text S1 in Supporting Information S1. Since the derivation of Equation 5 involves the particle approximations of C_i and its first-order derivatives, accuracy of Equation 5 depends on particle distributions, as discussed in Appendix A. For an irregular particle distribution, SPH accuracy improvement is needed.

2.2. C-SPH

The C-SPH has been developed to improve SPH accuracy for irregularly distributed particles by correcting the kernel gradient approximations (Chen & Beraum, 2000; Xu & Deng, 2016). To illustrate this method, we first apply the Taylor series expansion to $C_j = C(\mathbf{x}_j)$ at particle location $\mathbf{x}_i = \{x_i, y_i, z_i\}$, and retain the first-order derivatives, i.e.,

$$C_j \approx C_i + \left(\mathbf{x}_j^\alpha - \mathbf{x}_i^\alpha\right) \frac{\partial C_i}{\partial \mathbf{x}_i^\alpha} = C_i + (x_j - x_i) \frac{\partial C_i}{\partial x_i} + (y_j - y_i) \frac{\partial C_i}{\partial y_i} + (z_j - z_i) \frac{\partial C_i}{\partial z_i} \tag{6}$$

In C-SPH, the both sides of Taylor series expansion in Equation 6 are multiplied by the three first-order derivatives, $\partial W_{ij}/\partial x_i$, $\partial W_{ij}/\partial y_i$, and $\partial W_{ij}/\partial z_i$, and the results are integrated over the support domain. Subsequently, replacing the integrations with the particle approximations leads to

$$\begin{cases} \sum_{j=1}^{N_b} \frac{m_j}{\rho_j} C_j \frac{\partial W_{ij}}{\partial x_i} = \sum_{j=1}^{N_b} \frac{m_j}{\rho_j} C_i \frac{\partial W_{ij}}{\partial x_i} + \frac{\partial C_i}{\partial x_i} \sum_{j=1}^{N_b} \frac{m_j}{\rho_j} x_{ji} \frac{\partial W_{ij}}{\partial x_i} + \frac{\partial C_i}{\partial y_i} \sum_{j=1}^{N_b} \frac{m_j}{\rho_j} y_{ji} \frac{\partial W_{ij}}{\partial x_i} + \frac{\partial C_i}{\partial z_i} \sum_{j=1}^{N_b} \frac{m_j}{\rho_j} z_{ji} \frac{\partial W_{ij}}{\partial x_i} \\ \sum_{j=1}^{N_b} \frac{m_j}{\rho_j} C_j \frac{\partial W_{ij}}{\partial y_i} = \sum_{j=1}^{N_b} \frac{m_j}{\rho_j} C_i \frac{\partial W_{ij}}{\partial y_i} + \frac{\partial C_i}{\partial x_i} \sum_{j=1}^{N_b} \frac{m_j}{\rho_j} x_{ji} \frac{\partial W_{ij}}{\partial y_i} + \frac{\partial C_i}{\partial y_i} \sum_{j=1}^{N_b} \frac{m_j}{\rho_j} y_{ji} \frac{\partial W_{ij}}{\partial y_i} + \frac{\partial C_i}{\partial z_i} \sum_{j=1}^{N_b} \frac{m_j}{\rho_j} z_{ji} \frac{\partial W_{ij}}{\partial y_i} \\ \sum_{j=1}^{N_b} \frac{m_j}{\rho_j} C_j \frac{\partial W_{ij}}{\partial z_i} = \sum_{j=1}^{N_b} \frac{m_j}{\rho_j} C_i \frac{\partial W_{ij}}{\partial z_i} + \frac{\partial C_i}{\partial x_i} \sum_{j=1}^{N_b} \frac{m_j}{\rho_j} x_{ji} \frac{\partial W_{ij}}{\partial z_i} + \frac{\partial C_i}{\partial y_i} \sum_{j=1}^{N_b} \frac{m_j}{\rho_j} y_{ji} \frac{\partial W_{ij}}{\partial z_i} + \frac{\partial C_i}{\partial z_i} \sum_{j=1}^{N_b} \frac{m_j}{\rho_j} z_{ji} \frac{\partial W_{ij}}{\partial z_i} \end{cases} \tag{7}$$

where $x_{ji} = x_j - x_i$, $y_{ji} = y_j - y_i$ and $z_{ji} = z_j - z_i$. Moving the first term on the right-hand side of Equation 7 to the left-hand side gives

$$\begin{cases} \left\langle \frac{\partial C_i}{\partial x_i} \right\rangle = \sum_{j=1}^{N_b} \frac{m_j}{\rho_j} (C_j - C_i) \frac{\partial W_{ij}}{\partial x_i} = \frac{\partial C_i}{\partial x_i} \sum_{j=1}^{N_b} \frac{m_j}{\rho_j} x_{ji} \frac{\partial W_{ij}}{\partial x_i} + \frac{\partial C_i}{\partial y_i} \sum_{j=1}^{N_b} \frac{m_j}{\rho_j} y_{ji} \frac{\partial W_{ij}}{\partial x_i} + \frac{\partial C_i}{\partial z_i} \sum_{j=1}^{N_b} \frac{m_j}{\rho_j} z_{ji} \frac{\partial W_{ij}}{\partial x_i} \\ \left\langle \frac{\partial C_i}{\partial y_i} \right\rangle = \sum_{j=1}^{N_b} \frac{m_j}{\rho_j} (C_j - C_i) \frac{\partial W_{ij}}{\partial y_i} = \frac{\partial C_i}{\partial x_i} \sum_{j=1}^{N_b} \frac{m_j}{\rho_j} x_{ji} \frac{\partial W_{ij}}{\partial y_i} + \frac{\partial C_i}{\partial y_i} \sum_{j=1}^{N_b} \frac{m_j}{\rho_j} y_{ji} \frac{\partial W_{ij}}{\partial y_i} + \frac{\partial C_i}{\partial z_i} \sum_{j=1}^{N_b} \frac{m_j}{\rho_j} z_{ji} \frac{\partial W_{ij}}{\partial y_i} \\ \left\langle \frac{\partial C_i}{\partial z_i} \right\rangle = \sum_{j=1}^{N_b} \frac{m_j}{\rho_j} (C_j - C_i) \frac{\partial W_{ij}}{\partial z_i} = \frac{\partial C_i}{\partial x_i} \sum_{j=1}^{N_b} \frac{m_j}{\rho_j} x_{ji} \frac{\partial W_{ij}}{\partial z_i} + \frac{\partial C_i}{\partial y_i} \sum_{j=1}^{N_b} \frac{m_j}{\rho_j} y_{ji} \frac{\partial W_{ij}}{\partial z_i} + \frac{\partial C_i}{\partial z_i} \sum_{j=1}^{N_b} \frac{m_j}{\rho_j} z_{ji} \frac{\partial W_{ij}}{\partial z_i} \end{cases} \tag{8}$$

Rewriting Equation 8 into the matrix form, we have the particle approximations as

$$\begin{bmatrix} \left\langle \frac{\partial C_i}{\partial x_i} \right\rangle \\ \left\langle \frac{\partial C_i}{\partial y_i} \right\rangle \\ \left\langle \frac{\partial C_i}{\partial z_i} \right\rangle \end{bmatrix} = \begin{bmatrix} \sum_{j=1}^{N_b} \frac{m_j}{\rho_j} (C_j - C_i) \frac{\partial W_{ij}}{\partial x_i} \\ \sum_{j=1}^{N_b} \frac{m_j}{\rho_j} (C_j - C_i) \frac{\partial W_{ij}}{\partial y_i} \\ \sum_{j=1}^{N_b} \frac{m_j}{\rho_j} (C_j - C_i) \frac{\partial W_{ij}}{\partial z_i} \end{bmatrix} = \begin{bmatrix} \sum_{j=1}^{N_b} \frac{m_j}{\rho_j} x_{ji} \frac{\partial W_{ij}}{\partial x_i} & \sum_{j=1}^{N_b} \frac{m_j}{\rho_j} y_{ji} \frac{\partial W_{ij}}{\partial x_i} & \sum_{j=1}^{N_b} \frac{m_j}{\rho_j} z_{ji} \frac{\partial W_{ij}}{\partial x_i} \\ \sum_{j=1}^{N_b} \frac{m_j}{\rho_j} x_{ji} \frac{\partial W_{ij}}{\partial y_i} & \sum_{j=1}^{N_b} \frac{m_j}{\rho_j} y_{ji} \frac{\partial W_{ij}}{\partial y_i} & \sum_{j=1}^{N_b} \frac{m_j}{\rho_j} z_{ji} \frac{\partial W_{ij}}{\partial y_i} \\ \sum_{j=1}^{N_b} \frac{m_j}{\rho_j} x_{ji} \frac{\partial W_{ij}}{\partial z_i} & \sum_{j=1}^{N_b} \frac{m_j}{\rho_j} y_{ji} \frac{\partial W_{ij}}{\partial z_i} & \sum_{j=1}^{N_b} \frac{m_j}{\rho_j} z_{ji} \frac{\partial W_{ij}}{\partial z_i} \end{bmatrix} \begin{bmatrix} \frac{\partial C_i}{\partial x_i} \\ \frac{\partial C_i}{\partial y_i} \\ \frac{\partial C_i}{\partial z_i} \end{bmatrix} \tag{9}$$

This leads to the expression of the three first-order derivatives of C_i as

$$\begin{bmatrix} \frac{\partial C_i}{\partial x_i} \\ \frac{\partial C_i}{\partial y_i} \\ \frac{\partial C_i}{\partial z_i} \end{bmatrix} = \left(\mathbf{M}_i^C\right)^{-1} \begin{bmatrix} \sum_{j=1}^{N_b} \frac{m_j}{\rho_j} (C_j - C_i) \frac{\partial W_{ij}}{\partial x_i} \\ \sum_{j=1}^{N_b} \frac{m_j}{\rho_j} (C_j - C_i) \frac{\partial W_{ij}}{\partial y_i} \\ \sum_{j=1}^{N_b} \frac{m_j}{\rho_j} (C_j - C_i) \frac{\partial W_{ij}}{\partial z_i} \end{bmatrix} \tag{10}$$

where

$$\mathbf{M}_i^C = \begin{bmatrix} \sum_j \frac{m_j}{\rho_j} x_{ji} \frac{\partial W_{ij}}{\partial x_i} & \sum_j \frac{m_j}{\rho_j} y_{ji} \frac{\partial W_{ij}}{\partial x_i} & \sum_j \frac{m_j}{\rho_j} z_{ji} \frac{\partial W_{ij}}{\partial x_i} \\ \sum_j \frac{m_j}{\rho_j} x_{ji} \frac{\partial W_{ij}}{\partial y_i} & \sum_j \frac{m_j}{\rho_j} y_{ji} \frac{\partial W_{ij}}{\partial y_i} & \sum_j \frac{m_j}{\rho_j} z_{ji} \frac{\partial W_{ij}}{\partial y_i} \\ \sum_j \frac{m_j}{\rho_j} x_{ji} \frac{\partial W_{ij}}{\partial z_i} & \sum_j \frac{m_j}{\rho_j} y_{ji} \frac{\partial W_{ij}}{\partial z_i} & \sum_j \frac{m_j}{\rho_j} z_{ji} \frac{\partial W_{ij}}{\partial z_i} \end{bmatrix} \tag{11}$$

To transfer the modification in concentration derivatives to kernel gradient and to ensure that the antisymmetric property is satisfied, C-SPH assumes that there exists a modified kernel gradient, $\frac{\partial^{M_i^C} W_{ij}}{\partial \mathbf{x}_i}$. Using the modified kernel gradient and based on Equation 4, we can write the particle approximation of the first-order derivatives of C_i as

$$\left\langle \frac{\partial C_i}{\partial \mathbf{x}_i} \right\rangle = \sum_{j=1}^{N_b} \frac{m_j}{\rho_j} (C_j - C_i) \frac{\partial^{M_i^C} W_{ij}}{\partial \mathbf{x}_i} \tag{12}$$

Based on Equations 10 and 12, setting $\left\langle \frac{\partial C_i}{\partial \mathbf{x}_i} \right\rangle = \frac{\partial C_i}{\partial \mathbf{x}_i}$ gives

$$\begin{bmatrix} \sum_{j=1}^{N_b} \frac{m_j}{\rho_j} (C_j - C_i) \frac{\partial^{M_i^C} W_{ij}}{\partial x_i} \\ \sum_{j=1}^{N_b} \frac{m_j}{\rho_j} (C_j - C_i) \frac{\partial^{M_i^C} W_{ij}}{\partial y_i} \\ \sum_{j=1}^{N_b} \frac{m_j}{\rho_j} (C_j - C_i) \frac{\partial^{M_i^C} W_{ij}}{\partial z_i} \end{bmatrix} = \begin{bmatrix} \sum_{j=1}^{N_b} \frac{m_j}{\rho_j} x_{ji} \frac{\partial W_{ij}}{\partial x_i} & \sum_{j=1}^{N_b} \frac{m_j}{\rho_j} y_{ji} \frac{\partial W_{ij}}{\partial x_i} & \sum_{j=1}^{N_b} \frac{m_j}{\rho_j} z_{ji} \frac{\partial W_{ij}}{\partial x_i} \\ \sum_{j=1}^{N_b} \frac{m_j}{\rho_j} x_{ji} \frac{\partial W_{ij}}{\partial y_i} & \sum_{j=1}^{N_b} \frac{m_j}{\rho_j} y_{ji} \frac{\partial W_{ij}}{\partial y_i} & \sum_{j=1}^{N_b} \frac{m_j}{\rho_j} z_{ji} \frac{\partial W_{ij}}{\partial y_i} \\ \sum_{j=1}^{N_b} \frac{m_j}{\rho_j} x_{ji} \frac{\partial W_{ij}}{\partial z_i} & \sum_{j=1}^{N_b} \frac{m_j}{\rho_j} y_{ji} \frac{\partial W_{ij}}{\partial z_i} & \sum_{j=1}^{N_b} \frac{m_j}{\rho_j} z_{ji} \frac{\partial W_{ij}}{\partial z_i} \end{bmatrix}^{-1} \begin{bmatrix} \sum_{j=1}^{N_b} \frac{m_j}{\rho_j} (C_j - C_i) \frac{\partial W_{ij}}{\partial x_i} \\ \sum_{j=1}^{N_b} \frac{m_j}{\rho_j} (C_j - C_i) \frac{\partial W_{ij}}{\partial y_i} \\ \sum_{j=1}^{N_b} \frac{m_j}{\rho_j} (C_j - C_i) \frac{\partial W_{ij}}{\partial z_i} \end{bmatrix} \tag{13}$$

This leads to the modified kernel gradients as

$$\begin{bmatrix} \frac{\partial^{M_i^C} W_{ij}}{\partial x_i} \\ \frac{\partial^{M_i^C} W_{ij}}{\partial y_i} \\ \frac{\partial^{M_i^C} W_{ij}}{\partial z_i} \end{bmatrix} = \begin{bmatrix} \sum_{j=1}^{N_b} \frac{m_j}{\rho_j} x_{ji} \frac{\partial W_{ij}}{\partial x_i} & \sum_{j=1}^{N_b} \frac{m_j}{\rho_j} y_{ji} \frac{\partial W_{ij}}{\partial x_i} & \sum_{j=1}^{N_b} \frac{m_j}{\rho_j} z_{ji} \frac{\partial W_{ij}}{\partial x_i} \\ \sum_{j=1}^{N_b} \frac{m_j}{\rho_j} x_{ji} \frac{\partial W_{ij}}{\partial y_i} & \sum_{j=1}^{N_b} \frac{m_j}{\rho_j} y_{ji} \frac{\partial W_{ij}}{\partial y_i} & \sum_{j=1}^{N_b} \frac{m_j}{\rho_j} z_{ji} \frac{\partial W_{ij}}{\partial y_i} \\ \sum_{j=1}^{N_b} \frac{m_j}{\rho_j} x_{ji} \frac{\partial W_{ij}}{\partial z_i} & \sum_{j=1}^{N_b} \frac{m_j}{\rho_j} y_{ji} \frac{\partial W_{ij}}{\partial z_i} & \sum_{j=1}^{N_b} \frac{m_j}{\rho_j} z_{ji} \frac{\partial W_{ij}}{\partial z_i} \end{bmatrix}^{-1} \begin{bmatrix} \frac{\partial W_{ij}}{\partial x_i} \\ \frac{\partial W_{ij}}{\partial y_i} \\ \frac{\partial W_{ij}}{\partial z_i} \end{bmatrix} = \left(\mathbf{M}_i^C\right)^{-1} \begin{bmatrix} \frac{\partial W_{ij}}{\partial x_i} \\ \frac{\partial W_{ij}}{\partial y_i} \\ \frac{\partial W_{ij}}{\partial z_i} \end{bmatrix} \tag{14}$$

Expressing Equation 14 in a matrix form gives the modified kernel gradient as

$$\nabla_i^{M_i^C} W_{ij} = \left(\mathbf{M}_i^C\right)^{-1} \nabla_i W_{ij} \tag{15}$$

With this modified kernel gradient, in C-SPH, the gradient of concentration is approximated by using Equation 15 rather than Equation 4, so that the antisymmetric property of kernel first-order derivatives is satisfied.

Following Xu and Deng (2016), we derive the C-SPH solution of ADE. This is done by replacing kernel gradient $\nabla_i W_{ij}$ in Equation 5 with the modified kernel gradient, $\nabla_i^{M_i^C} W_{ij}$, corrected by using matrix $\mathbf{M}_i^C$. The correction made to the kernel gradient is also suitable to the SPH approximation of the dispersion term, because the second-order derivative in the dispersive term of Equation 2 is evaluated by a hybrid expression of SPH first-order derivative and a finite difference approximation of the first-order derivative, as discussed in Section 2.1. Correcting the kernel gradient helps satisfy the antisymmetric property of the first-order derivative as discussed in Text

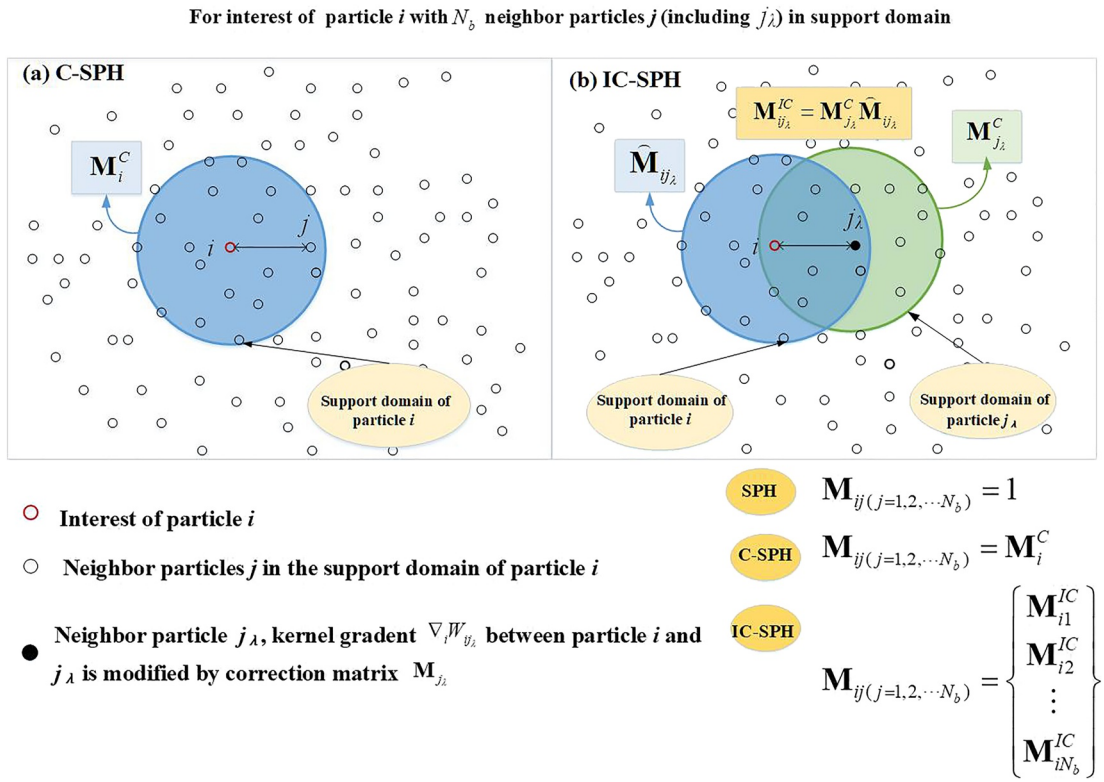

Figure 1. Sketches of correction matrix **M** in (a) Corrected Smoothed Particle Hydrodynamics (C-SPH) and (b) Interactively Corrected Smoothed Particle Hydrodynamics (IC-SPH) methods for particle *i* in a two-dimensional space. For standard SPH, no correction is made to a kernel gradient, and **M** is an identity matrix. For C-SPH, correction matrix $\mathbf{M}_i^C$ is based on the particle in the support domain of particle *i*. For IC-SPH, correction matrix $\mathbf{M}_{ij}^{IC}$ is based not only on particles in the support domain of particle *i* but also on particles within the support domain of particle *j*, a neighbor particle of particle *i*.

S1 in Supporting Information S1, which in turn helps improve accuracy of the first-order derivative of concentration and accuracy of the dispersion term approximation in Equation 5 with irregularly distributed particles. This is an advantage of C-SPH, because C-SPH solution of the ADE can be implemented in a straightforward way based on Equation 5 of the SPH implementation without significantly changing the SPH implementation codes. This has been done in several studies (Ren et al., 2011, 2015; Zhu et al., 2018). With the corrected kernel gradient, the C-SPH is less sensitive to particle irregularity. When $\mathbf{M}_i^C$ is a unity matrix, the C-SPH implementation is identical to the SPH implementation.

In C-SPH, since the correction to the first-order derivatives of concentration is made directly to the kernel gradients (Equation 15), the correction matrix $\mathbf{M}_i^C$ used to modify kernel gradient $\nabla_i W_{ij}$ in Equation 15 is the same for all neighbor particles *j* in the support domain of particle *i*, as shown in Figure 1a. In other words, $\mathbf{M}_i^C$ only uses the particles within the support domain of particle *i*, and does not consider the particles within the support domain of particle *j*. Since kernel function W_{ij} and its gradient $\nabla_i W_{ij}$ are jointly determined by particles *i* and *j*, the particles within the support domain of particle *j* should be used to correct the kernel gradient at particle *i*. Following this idea, IC-SPH corrects the kernel gradient $\nabla_i W_{ij}$ by considering the particles within the support domains of both particles *i* and *j*. This is the key idea behind IC-SPH.

2.3. IC-SPH

To derive IC-SPH, we choose kernel gradient $\frac{\partial W_{ij_\lambda}}{\partial \mathbf{x}_i}$ as an example to construct a system of equations whose solutions are the interactively corrected kernel gradient $\frac{\partial^{M_{ij_\lambda}^{IC}} W_{ij_\lambda}}{\partial \mathbf{x}_i}$. Figure 1b uses a filled circle to show the location of particle j_λ, where subscript $\lambda = 1, 2, \ldots, N_b$ is the index of particle *j* within the support domain of particle *i* and N_b is the number of neighbor particles within the support domain of particle *i*. Using particle j_λ to illustrate the

process of correcting kernel gradient $\frac{\partial W_{ij_\lambda}}{\partial \mathbf{x}_i}$, we first construct three vectors $\mathbf{L}_{\lambda x}$, $\mathbf{L}_{\lambda y}$, and $\mathbf{L}_{\lambda z}$ for a three-dimensional problem, as a partially modified kernel gradient is only for particle j_λ. The three vectors are similar, taking the x direction vector of $\mathbf{L}_{\lambda x}$ as an example, its vector form is $\mathbf{L}_{\lambda x} = \left[-\frac{\partial W_{ij_1}}{\partial x_{j_1}} \quad \cdots \quad -\frac{\partial^{M^C_{j_\lambda}} W_{ij_\lambda}}{\partial x_{j_\lambda}} \quad \cdots \quad -\frac{\partial W_{ij_{N_b}}}{\partial x_{j_{N_b}}} \right]^T$, where $-\frac{\partial^{M^C_{j_\lambda}} W_{ij_\lambda}}{\partial x_{j_\lambda}}$ is the corrected first-order derivative of the kernel function that is modified by correction matrix $\mathbf{M}_{j_\lambda}$, i.e., $\frac{\partial^{M^C_{j_\lambda}} W_{ij_\lambda}}{\partial x_{j_\lambda}} = \left(\mathbf{M}^C_{j_\lambda}\right)^{-1} \frac{\partial W_{ij_\lambda}}{\partial x_{j_\lambda}}$. The $-\frac{\partial^{M^C_{j_\lambda}} W_{ij_\lambda}}{\partial x_{j_\lambda}}$ term implies that the kernel gradient between particles i and j_λ is modified by correction matrix $\mathbf{M}_{j_\lambda}$. Subsequently, we multiply $\mathbf{L}_{\lambda x}$, $\mathbf{L}_{\lambda y}$, and $\mathbf{L}_{\lambda z}$ to the both sides of Equation 6, and then integrate them over the support domain. Replacing the integrations with the particle approximations leads to a system of equations similar to Equation 8 in the vector multiplication form as

$$\begin{cases} \left\langle \frac{\partial C_i}{\partial x_i} \right\rangle = \left[\frac{m_{j_1}}{\rho_{j_1}} \left(C_{j_1} - C_i\right) \quad \frac{m_{j_2}}{\rho_{j_2}} \left(C_{j_2} - C_i\right) \quad \cdots \quad \frac{m_{j_{N_b}}}{\rho_{j_{N_b}}} \left(C_{j_{N_b}} - C_i\right) \right] \mathbf{L}_{\lambda x} = \frac{\partial C_i}{\partial x_i} \mathbf{P}_x \mathbf{L}_{\lambda x} + \frac{\partial C_i}{\partial y_i} \mathbf{P}_y \mathbf{L}_{\lambda x} + \frac{\partial C_i}{\partial z_i} \mathbf{P}_z \mathbf{L}_{\lambda x} \\ \left\langle \frac{\partial C_i}{\partial y_i} \right\rangle = \left[\frac{m_{j_1}}{\rho_{j_1}} \left(C_{j_1} - C_i\right) \quad \frac{m_{j_2}}{\rho_{j_2}} \left(C_{j_2} - C_i\right) \quad \cdots \quad \frac{m_{j_{N_b}}}{\rho_{j_{N_b}}} \left(C_{j_{N_b}} - C_i\right) \right] \mathbf{L}_{\lambda y} = \frac{\partial C_i}{\partial x_i} \mathbf{P}_x \mathbf{L}_{\lambda y} + \frac{\partial C_i}{\partial y_i} \mathbf{P}_y \mathbf{L}_{\lambda y} + \frac{\partial C_i}{\partial z_i} \mathbf{P}_z \mathbf{L}_{\lambda y} \\ \left\langle \frac{\partial C_i}{\partial z_i} \right\rangle = \left[\frac{m_{j_1}}{\rho_{j_1}} \left(C_{j_1} - C_i\right) \quad \frac{m_{j_2}}{\rho_{j_2}} \left(C_{j_2} - C_i\right) \quad \cdots \quad \frac{m_{j_{N_b}}}{\rho_{j_{N_b}}} \left(C_{j_{N_b}} - C_i\right) \right] \mathbf{L}_{\lambda z} = \frac{\partial C_i}{\partial x_i} \mathbf{P}_x \mathbf{L}_{\lambda z} + \frac{\partial C_i}{\partial y_i} \mathbf{P}_y \mathbf{L}_{\lambda z} + \frac{\partial C_i}{\partial z_i} \mathbf{P}_z \mathbf{L}_{\lambda z} \end{cases} \tag{16}$$

where $\mathbf{P}_\mathbf{x} = \left[\left(m_{j_1}/\rho_{j_1}\right)\left(\mathbf{x}_{j_1} - \mathbf{x}_i\right) \quad \left(m_{j_2}/\rho_{j_2}\right)\left(\mathbf{x}_{j_2} - \mathbf{x}_i\right) \quad \cdots \quad \left(m_{j_{N_b}}/\rho_{j_{N_b}}\right)\left(\mathbf{x}_{j_{N_b}} - \mathbf{x}_i\right) \right]$ for $\mathbf{x} = \{x, y, z\}$. Rewrite the last terms of Equation 16 in a matrix form as

$$\begin{aligned} \begin{bmatrix} \left\langle \frac{\partial C_i}{\partial x_i} \right\rangle \\ \left\langle \frac{\partial C_i}{\partial y_i} \right\rangle \\ \left\langle \frac{\partial C_i}{\partial z_i} \right\rangle \end{bmatrix} &= \begin{bmatrix} \left[\frac{m_{j_1}}{\rho_{j_1}} \left(C_{j_1} - C_i\right) \quad \frac{m_{j_2}}{\rho_{j_2}} \left(C_{j_2} - C_i\right) \quad \cdots \quad \frac{m_{j_{N_b}}}{\rho_{j_{N_b}}} \left(C_{j_{N_b}} - C_i\right) \right] \mathbf{L}_{\lambda x} \\ \left[\frac{m_{j_1}}{\rho_{j_1}} \left(C_{j_1} - C_i\right) \quad \frac{m_{j_2}}{\rho_{j_2}} \left(C_{j_2} - C_i\right) \quad \cdots \quad \frac{m_{j_{N_b}}}{\rho_{j_{N_b}}} \left(C_{j_{N_b}} - C_i\right) \right] \mathbf{L}_{\lambda y} \\ \left[\frac{m_{j_1}}{\rho_{j_1}} \left(C_{j_1} - C_i\right) \quad \frac{m_{j_2}}{\rho_{j_2}} \left(C_{j_2} - C_i\right) \quad \cdots \quad \frac{m_{j_{N_b}}}{\rho_{j_{N_b}}} \left(C_{j_{N_b}} - C_i\right) \right] \mathbf{L}_{\lambda z} \end{bmatrix} \\ &= \begin{bmatrix} \mathbf{P}_x \mathbf{L}_{\lambda x} & \mathbf{P}_y \mathbf{L}_{\lambda x} & \mathbf{P}_z \mathbf{L}_{\lambda x} \\ \mathbf{P}_x \mathbf{L}_{\lambda y} & \mathbf{P}_y \mathbf{L}_{\lambda y} & \mathbf{P}_z \mathbf{L}_{\lambda y} \\ \mathbf{P}_x \mathbf{L}_{\lambda z} & \mathbf{P}_y \mathbf{L}_{\lambda z} & \mathbf{P}_z \mathbf{L}_{\lambda z} \end{bmatrix} \begin{bmatrix} \frac{\partial C_i}{\partial x_i} \\ \frac{\partial C_i}{\partial y_i} \\ \frac{\partial C_i}{\partial z_i} \end{bmatrix} \end{aligned} \tag{17}$$

This leads to

$$\begin{bmatrix} \frac{\partial C_i}{\partial x_i} \\ \frac{\partial C_i}{\partial y_i} \\ \frac{\partial C_i}{\partial z_i} \end{bmatrix} = \begin{bmatrix} \mathbf{P}_x \mathbf{L}_{\lambda x} & \mathbf{P}_y \mathbf{L}_{\lambda x} & \mathbf{P}_z \mathbf{L}_{\lambda x} \\ \mathbf{P}_x \mathbf{L}_{\lambda y} & \mathbf{P}_y \mathbf{L}_{\lambda y} & \mathbf{P}_z \mathbf{L}_{\lambda y} \\ \mathbf{P}_x \mathbf{L}_{\lambda z} & \mathbf{P}_y \mathbf{L}_{\lambda z} & \mathbf{P}_z \mathbf{L}_{\lambda z} \end{bmatrix}^{-1} \begin{bmatrix} \left[\frac{m_{j_1}}{\rho_{j_1}} \left(C_{j_1} - C_i\right) \quad \frac{m_{j_2}}{\rho_{j_2}} \left(C_{j_2} - C_i\right) \quad \cdots \quad \frac{m_{j_{N_b}}}{\rho_{j_{N_b}}} \left(C_{j_{N_b}} - C_i\right) \right] \mathbf{L}_{\lambda x} \\ \left[\frac{m_{j_1}}{\rho_{j_1}} \left(C_{j_1} - C_i\right) \quad \frac{m_{j_2}}{\rho_{j_2}} \left(C_{j_2} - C_i\right) \quad \cdots \quad \frac{m_{j_{N_b}}}{\rho_{j_{N_b}}} \left(C_{j_{N_b}} - C_i\right) \right] \mathbf{L}_{\lambda y} \\ \left[\frac{m_{j_1}}{\rho_{j_1}} \left(C_{j_1} - C_i\right) \quad \frac{m_{j_2}}{\rho_{j_2}} \left(C_{j_2} - C_i\right) \quad \cdots \quad \frac{m_{j_{N_b}}}{\rho_{j_{N_b}}} \left(C_{j_{N_b}} - C_i\right) \right] \mathbf{L}_{\lambda z} \end{bmatrix} \tag{18}$$

To derive the modified kernel gradients of IC-SPH with particles within the support domains of particles i and j, we follow the C-SPH method to assume that there exists a modified kernel gradient denoted as $\mathbf{L}^M_{\lambda\mathbf{x}}$. Based on Equation 4, we can write the particle approximation of the first-order derivatives of C_i as

$$\left\langle \frac{\partial C_i}{\partial \mathbf{x}_i} \right\rangle = \left[\frac{m_{j_1}}{\rho_{j_1}} \left(C_{j_1} - C_i\right) \quad \frac{m_{j_2}}{\rho_{j_2}} \left(C_{j_2} - C_i\right) \quad \cdots \quad \frac{m_{j_{N_b}}}{\rho_{j_{N_b}}} \left(C_{j_{N_b}} - C_i\right) \right] \times \mathbf{L}^M_{\lambda\mathbf{x}} \tag{19}$$

where $\mathbf{L}^M_{\lambda\mathbf{x}} = \left[\frac{\partial^{\widehat{M}_{ij}} W_{ij_1}}{\partial \mathbf{x}_i} \quad \cdots \quad \frac{\partial^{M^{IC}_{ij_\lambda}} W_{ij_\lambda}}{\partial \mathbf{x}_i} \quad \cdots \quad \frac{\partial^{\widehat{M}_{ij_{N_b}}} W_{ij_{N_b}}}{\partial \mathbf{x}_i} \right]^T$ for $\mathbf{x} = \{x, y, z\}$. Setting $\left\langle \frac{\partial C_i}{\partial \mathbf{x}_i} \right\rangle = \frac{\partial C_i}{\partial \mathbf{x}_i}$ based on Equations 18 and 19 gives

$$
\begin{bmatrix}
\left[\frac{m_{j_1}}{\rho_{j_1}}\left(C_{j_1}-C_i\right) & \frac{m_{j_2}}{\rho_{j_2}}\left(C_{j_2}-C_i\right) & \cdots & \frac{m_{j_{N_b}}}{\rho_{j_{N_b}}}\left(C_{j_{N_b}}-C_i\right)\right]\mathbf{L}^M_{\lambda x}\\
\left[\frac{m_{j_1}}{\rho_{j_1}}\left(C_{j_1}-C_i\right) & \frac{m_{j_2}}{\rho_{j_2}}\left(C_{j_2}-C_i\right) & \cdots & \frac{m_{j_{N_b}}}{\rho_{j_{N_b}}}\left(C_{j_{N_b}}-C_i\right)\right]\mathbf{L}^M_{\lambda y}\\
\left[\frac{m_{j_1}}{\rho_{j_1}}\left(C_{j_1}-C_i\right) & \frac{m_{j_2}}{\rho_{j_2}}\left(C_{j_2}-C_i\right) & \cdots & \frac{m_{j_{N_b}}}{\rho_{j_{N_b}}}\left(C_{j_{N_b}}-C_i\right)\right]\mathbf{L}^M_{\lambda z}
\end{bmatrix}
$$

$$
=\begin{bmatrix}
\mathbf{P}_x\mathbf{L}_{\lambda x} & \mathbf{P}_y\mathbf{L}_{\lambda x} & \mathbf{P}_z\mathbf{L}_{\lambda x}\\
\mathbf{P}_x\mathbf{L}_{\lambda y} & \mathbf{P}_y\mathbf{L}_{\lambda y} & \mathbf{P}_z\mathbf{L}_{\lambda y}\\
\mathbf{P}_x\mathbf{L}_{\lambda z} & \mathbf{P}_y\mathbf{L}_{\lambda z} & \mathbf{P}_z\mathbf{L}_{\lambda z}
\end{bmatrix}^{-1}
\begin{bmatrix}
\left[\frac{m_{j_1}}{\rho_{j_1}}\left(C_{j_1}-C_i\right) & \frac{m_{j_2}}{\rho_{j_2}}\left(C_{j_2}-C_i\right) & \cdots & \frac{m_{j_{N_b}}}{\rho_{j_{N_b}}}\left(C_{j_{N_b}}-C_i\right)\right]\mathbf{L}_{\lambda x}\\
\left[\frac{m_{j_1}}{\rho_{j_1}}\left(C_{j_1}-C_i\right) & \frac{m_{j_2}}{\rho_{j_2}}\left(C_{j_2}-C_i\right) & \cdots & \frac{m_{j_{N_b}}}{\rho_{j_{N_b}}}\left(C_{j_{N_b}}-C_i\right)\right]\mathbf{L}_{\lambda y}\\
\left[\frac{m_{j_1}}{\rho_{j_1}}\left(C_{j_1}-C_i\right) & \frac{m_{j_2}}{\rho_{j_2}}\left(C_{j_2}-C_i\right) & \cdots & \frac{m_{j_{N_b}}}{\rho_{j_{N_b}}}\left(C_{j_{N_b}}-C_i\right)\right]\mathbf{L}_{\lambda z}
\end{bmatrix} \tag{20}
$$

This leads to the modified kernel gradients as

$$
\begin{bmatrix}\mathbf{L}^M_{\lambda x}\\ \mathbf{L}^M_{\lambda y}\\ \mathbf{L}^M_{\lambda z}\end{bmatrix}=\begin{bmatrix}\mathbf{P}_x\mathbf{L}_{\lambda x} & \mathbf{P}_y\mathbf{L}_{\lambda x} & \mathbf{P}_z\mathbf{L}_{\lambda x}\\ \mathbf{P}_x\mathbf{L}_{\lambda y} & \mathbf{P}_y\mathbf{L}_{\lambda y} & \mathbf{P}_z\mathbf{L}_{\lambda y}\\ \mathbf{P}_x\mathbf{L}_{\lambda z} & \mathbf{P}_y\mathbf{L}_{\lambda z} & \mathbf{P}_z\mathbf{L}_{\lambda z}\end{bmatrix}^{-1}\begin{bmatrix}\mathbf{L}_{\lambda x}\\ \mathbf{L}_{\lambda y}\\ \mathbf{L}_{\lambda z}\end{bmatrix}=\widehat{\mathbf{M}}_{ij_\lambda}{}^{-1}\begin{bmatrix}\mathbf{L}_{\lambda x}\\ \mathbf{L}_{\lambda y}\\ \mathbf{L}_{\lambda z}\end{bmatrix} \tag{21}
$$

The elements in $\mathbf{L}^M_{\lambda\mathbf{x}}$ and $\mathbf{L}_{\lambda\mathbf{x}}$ are all kernel gradients. Then based on Equation 21, for the j_λth particle, the interactively corrected kernel gradient is given as

$$
\nabla_i^{M^{IC}_{ij_\lambda}} W_{ij_\lambda}=\widehat{\mathbf{M}}_{ij_\lambda}{}^{-1}\left(-\nabla_{j_\lambda}^{M^C_{j_\lambda}} W_{ij_\lambda}\right) \tag{22}
$$

where the corrected kernel gradient at particle j_λ is based on Equation 15, i.e.,

$$
\nabla_{j_\lambda}^{M^C_{j_\lambda}} W_{ij_\lambda}=\left(\mathbf{M}^C_{j_\lambda}\right)^{-1}\nabla_{j_\lambda} W_{ij_\lambda} \tag{23}
$$

where $\mathbf{M}^C_{j_\lambda}$ is given as

$$
\mathbf{M}^C_{j_\lambda}=\begin{bmatrix}
\sum_k \frac{m_k}{\rho_k}x_{kj_\lambda}\frac{\partial W_{j_\lambda k}}{\partial x_{j_\lambda}} & \sum_k \frac{m_k}{\rho_k}y_{kj_\lambda}\frac{\partial W_{j_\lambda k}}{\partial x_{j_\lambda}} & \sum_k \frac{m_k}{\rho_k}z_{kj_\lambda}\frac{\partial W_{j_\lambda k}}{\partial x_{j_\lambda}}\\
\sum_k \frac{m_k}{\rho_k}x_{kj_\lambda}\frac{\partial W_{j_\lambda k}}{\partial y_{j_\lambda}} & \sum_k \frac{m_k}{\rho_k}y_{kj_\lambda}\frac{\partial W_{j_\lambda k}}{\partial y_{j_\lambda}} & \sum_k \frac{m_k}{\rho_k}z_{kj_\lambda}\frac{\partial W_{j_\lambda k}}{\partial y_{j_\lambda}}\\
\sum_k \frac{m_k}{\rho_k}x_{kj_\lambda}\frac{\partial W_{j_\lambda k}}{\partial z_{j_\lambda}} & \sum_k \frac{m_k}{\rho_k}y_{kj_\lambda}\frac{\partial W_{j_\lambda k}}{\partial z_{j_\lambda}} & \sum_k \frac{m_k}{\rho_k}z_{kj_\lambda}\frac{\partial W_{j_\lambda k}}{\partial z_{j_\lambda}}
\end{bmatrix} \tag{24}
$$

$x_{kj_\lambda}=x_k-x_{j_\lambda}$, $y_{kj_\lambda}=y_k-y_{j_\lambda}$, and $z_{kj_\lambda}=z_k-z_{j_\lambda}$, and particles k are the neighbor particles of particle j_λ. Matrix $\widehat{\mathbf{M}}_{ij_\lambda}$ in Equation 22 is given as

$$
\widehat{\mathbf{M}}_{ij_\lambda}=\begin{bmatrix}\mathbf{P}_x\mathbf{L}_{\lambda x} & \mathbf{P}_y\mathbf{L}_{\lambda x} & \mathbf{P}_z\mathbf{L}_{\lambda x}\\ \mathbf{P}_x\mathbf{L}_{\lambda y} & \mathbf{P}_y\mathbf{L}_{\lambda y} & \mathbf{P}_z\mathbf{L}_{\lambda y}\\ \mathbf{P}_x\mathbf{L}_{\lambda z} & \mathbf{P}_y\mathbf{L}_{\lambda z} & \mathbf{P}_z\mathbf{L}_{\lambda z}\end{bmatrix} \tag{25}
$$

$$
=\begin{bmatrix}
\frac{m_{j_\lambda}}{\rho_{j_\lambda}}x_{j_\lambda i}\left(-\frac{\partial^{M_{j_\lambda}}W_{ij_\lambda}}{\partial x_{j_\lambda}}\right)+\sum_{j\neq j_\lambda}\frac{m_j}{\rho_j}x_{ji}\frac{\partial W_{ij}}{\partial x_i}\frac{m_{j_\lambda}}{\rho_{j_\lambda}}y_{j_\lambda i}\left(\frac{\partial^{M_{j_\lambda}}W_{ij_\lambda}}{\partial x_{j_\lambda}}\right)+\sum_{j\neq j_\lambda}\frac{m_j}{\rho_j}y_{ji}\frac{\partial W_{ij}}{\partial x_i} & \frac{m_{j_\lambda}}{\rho_{j_\lambda}}z_{j_\lambda i}\left(\frac{\partial^{M_{j_\lambda}}W_{ij_\lambda}}{\partial x_{j_\lambda}}\right)+\sum_{j\neq j_\lambda}\frac{m_j}{\rho_j}z_{ji}\frac{\partial W_{ij}}{\partial x_i}\\
\frac{m_{j_\lambda}}{\rho_{j_\lambda}}x_{j_\lambda i}\left(-\frac{\partial^{M_{j_\lambda}}W_{ij_\lambda}}{\partial y_{j_\lambda}}\right)+\sum_{j\neq j_\lambda}\frac{m_j}{\rho_j}x_{ji}\frac{\partial W_{ij}}{\partial y_i}\frac{m_{j_\lambda}}{\rho_{j_\lambda}}y_{j_\lambda i}\left(-\frac{\partial^{M_{j_\lambda}}W_{ij_\lambda}}{\partial y_{j_\lambda}}\right)+\sum_{j\neq j_\lambda}\frac{m_j}{\rho_j}y_{ji}\frac{\partial W_{ij}}{\partial y_i} & \frac{m_{j_\lambda}}{\rho_{j_\lambda}}z_{j_\lambda i}\left(-\frac{\partial^{M_{j_\lambda}}W_{ij_\lambda}}{\partial y_{j_\lambda}}\right)+\sum_{j\neq j_\lambda}\frac{m_j}{\rho_j}z_{ji}\frac{\partial W_{ij}}{\partial y_i}\\
\frac{m_{j_\lambda}}{\rho_{j_\lambda}}x_{j_\lambda i}\left(-\frac{\partial^{M_{j_\lambda}}W_{ij_\lambda}}{\partial z_{j_\lambda}}\right)+\sum_{j\neq j_\lambda}\frac{m_j}{\rho_j}x_{ji}\frac{\partial W_{ij}}{\partial z_i}\frac{m_{j_\lambda}}{\rho_{j_\lambda}}y_{j_\lambda i}\left(-\frac{\partial^{M_{j_\lambda}}W_{ij_\lambda}}{\partial z_{j_\lambda}}\right)+\sum_{j\neq j_\lambda}\frac{m_j}{\rho_j}y_{ji}\frac{\partial W_{ij}}{\partial z_i} & \frac{m_{j_\lambda}}{\rho_{j_\lambda}}z_{j_\lambda i}\left(-\frac{\partial^{M_{j_\lambda}}W_{ij_\lambda}}{\partial z_{j_\lambda}}\right)+\sum_{j\neq j_\lambda}\frac{m_j}{\rho_j}z_{ji}\frac{\partial W_{ij}}{\partial z_i}
\end{bmatrix}
$$

Note that the only difference between matrix $\widehat{\mathbf{M}}_{ij_\lambda}$ in Equation 25 and $\mathbf{M}_i^C$ in Equation 11 is the element of specific particle j_λ in the kernel gradient.

Since $-\nabla_j W_{ij} = \nabla_i W_{ij}$ in SPH, the unmodified kernel gradients at particles $\sim j_\lambda$ (all particles except j_λ in the support domain of particle i) in $\mathbf{L}_{\lambda\mathbf{x}}$ can be replaced by the kernel gradient at particle i with an opposite sign. Based on the two correction matrices $\mathbf{M}_{j_\lambda}^C$ and $\widehat{\mathbf{M}}_{ij_\lambda}$, the interactively corrected kernel gradient at particle i determined by particle i and j_λ can be written as

$$\begin{aligned}\nabla_i^{M_{ij_\lambda}^{IC}} W_{ij_\lambda} = \widehat{\mathbf{M}}_{ij_\lambda}^{-1}\left(-\nabla_{j_\lambda}^{M_{j_\lambda}^C} W_{ij_\lambda}\right) &= \widehat{\mathbf{M}}_{ij_\lambda}^{-1}\left(-\left(\mathbf{M}_{j_\lambda}^C\right)^{-1}\nabla_{j_\lambda} W_{ij_\lambda}\right)\\ &= \left(\widehat{\mathbf{M}}_{ij_\lambda}^{-1}\left(\mathbf{M}_{j_\lambda}^C\right)^{-1}\nabla_i W_{ij_\lambda}\right) = \left(\mathbf{M}_{ij_\lambda}^{IC}\right)^{-1}\nabla_i W_{ij_\lambda}\end{aligned} \tag{26}$$

The interactive correction matrix, $\mathbf{M}_{ij_\lambda}^{IC}$, is defined for the j_λth particle as

$$\mathbf{M}_{ij_\lambda}^{IC} = \mathbf{M}_{j_\lambda}^C\,\widehat{\mathbf{M}}_{ij_\lambda} \tag{27}$$

where matrices $\mathbf{M}_{j_\lambda}^C$ and $\widehat{\mathbf{M}}_{ij_\lambda}$ are given in Equations 24 and 25, respectively. For particle i with N_b neighbor particles in its support domain, we need to construct N_b systems of equations of 16 and solve them to derive the interactively corrected kernel gradient. Accordingly, we have N_b correction matrices $\mathbf{M}_{ij_\lambda}^{IC}$.

Figure 1b illustrates the relations between the three matrices above. For particle i and its support domain in blue, we can construct matrix $\widehat{\mathbf{M}}_{ij_\lambda}$, which is similar to $\mathbf{M}_i^C$ used in C-SPH except for particle j_λ. For this particle and its support domain in green, we can construct matrix $\mathbf{M}_{j_\lambda}^C$, which is equivalent to $\mathbf{M}_i^C$ but for interest particle of j_λ. Using $\widehat{\mathbf{M}}_{ij_\lambda}$ and $\mathbf{M}_{j_\lambda}^C$, we have $\mathbf{M}_{ij_\lambda}^{IC}$. For particle i with N_b neighbor particles in its support domain, since each particle j_λ has its own matrix $\mathbf{M}_{j_\lambda}^C$, and matrix $\mathbf{M}_{ij_\lambda}^{IC}$ may be different for different particle j_λ. Constructing matrix $\mathbf{M}_{ij_\lambda}^{IC}$ is the key component of IC-SPH, and it embraces two steps of corrections, one for particle i and the other for particle j_λ. The latter correction is an advantage of IC-SPH, because it can reduce the smoothing and discretizing errors associated with particle j_λ.

For generality, we drop λ, and use $\mathbf{M}_{ij}^{IC}$ to represent the correction matrix for any neighbor particles j within the support domain of particle i. Thus, similar to Equation 15 for C-SPH, the interactively corrected kernel gradient is given as

$$\nabla_i^{M_{ij}^{IC}} W_{ij} = \left(\mathbf{M}_{ij}^{IC}\right)^{-1}\nabla_i W_{ij} \tag{28}$$

In IC-SPH, the correction matrix $\mathbf{M}_i^C$ of C-SPH is replaced by $\mathbf{M}_{ij}^{IC}$. With Equation 28, replacing kernel gradient $\nabla_i W_{ij}$ in Equation 5 with the modified kernel gradient $\nabla_i^{M_{ij}^{IC}} W_{ij}$ corrected by using matrix $\mathbf{M}_{ij}^{IC}$ gives the IC-SPH solution of the ADE as

$$\frac{dC_i}{dt} = \frac{1}{2}\sum_{j=1}^{N_b}\frac{1}{n_{ij}}\left(C_j - C_i\right)D_{ij}\frac{\mathbf{x}_j - \mathbf{x}_i}{|\mathbf{x}_j - \mathbf{x}_i|^2}\cdot\nabla_i^{M_{ij}^{IC}} W_{ij} \tag{29}$$

The only difference between Equations 5 and 29 is the use of the interactively modified kernel gradient corrected by using matrix $\mathbf{M}_{ij}^{IC}$. The reason is similar to that in C-SPH method has been discussed in Section 2.2. This is an advantage of IC-SPH, because Equation 29 can be implemented in a straightforward way based on Equation 5 of the SPH implementation. When $\mathbf{M}_j^C$ is a unity matrix (i.e., no correction is needed for neighbor particle j), the IC-SPH implementation is identical to the C-SPH implementation; when $\mathbf{M}_j^C$ and $\widehat{\mathbf{M}}_{ij}$ matrices are both unity matrices (i.e., no correction is needed for both particles i and j), $\mathbf{M}_{ij}^{IC} = \mathbf{M}_j^C\,\widehat{\mathbf{M}}_{ij}$ is a unity matrix, the IC-SPH implementation is identical to the SPH implementation.

This study estimates the modified kernel gradient, $\nabla_i^{M_{ij}^{IC}} W_{ij}$, by solving the system of equations, $\mathbf{M}_{ij}^{IC}\nabla_i^{M_{ij}^{IC}} W_{ij} = \nabla_i W_{ij}$ in two steps first for $\mathbf{M}_j^C\nabla_i^{M_j^C} W_{ij} = \nabla_i W_{ij}$ and then for $\widehat{\mathbf{M}}_{ij}\,\nabla_i^{M_{ij}^{IC}} W_{ij} = \nabla_i^{M_j^C} W_{ij}$. Since IC-SPH needs to solve two systems of equations to obtain the modified kernel gradient, IC-SPH is computation-

ally more expensive than both SPH and C-SPH that only need to solve one system of equations. A comparison of the CPU times for the three methods are given in Sections 3.1.2 and 3.2.2 for two numerical examples. If matrix $\mathbf{M}_{ij}^{IC}$ is ill-conditioned or even singular for cases with highly irregular particles, IC-SPH may suffer from numerical instability or early termination. This occurs in the numerical experiments shown in Section 3 where IC-SPH is used to simulate a solute transport problem with irregular particle distributions. To resolve this problem, following the decoupled finite particle method developed by Zhang and Liu (2018), we use the decoupled IC-SPH, and replace $\mathbf{M}_{ij}^{IC}$ by the diagonal matrix $\overline{\mathbf{M}}_{ij}^{IC}$ that only contains the diagonal elements of $\mathbf{M}_{ij}^{IC}$. This is under the assumptions that the contribution of correction from the self-direction is dominant and that the contributions from other directions are negligible. This is similar to the estimation of partial derivatives in finite difference methods, in which a partial derivative in one direction is frequently replaced by a finite differencing along the same direction. In this study, if $\mathbf{M}_{ij}^{IC}\nabla_i^{M_{ij}^{IC}} W_{ij} = \nabla_i W_{ij}$ cannot be solved due to ill-conditioned $\mathbf{M}_{ij}^{IC}$, the decoupled IC-SPH is used.

2.4. Error With Irregular Particle Distribution

According to Monaghan (2005), meshless approximations based on a kernel interpolant integration have two sources of numerical errors as follows: (a) the smoothing error caused by integral interpolation, which depends on the shape and smoothing length of the kernel function, and (b) numerical discretizing error caused by summation of discrete particles in the integral, which depends upon the number and location of the particles. To simultaneously reduce smoothing and discretizing errors requires decreasing the smoothing length and simultaneously increasing the number of particles, so that the number of particles per support domain does not change on an average sense for all particles (Zhu et al., 2015). This, however, is difficult to achieve for an irregular particle distribution, because it is difficult to estimate the number of particles within a support domain for irregularly distributed particles (Herrera et al., 2009).

When using SPH, C-SPH, or IC-SPH to solve ADE with heterogeneous hydraulic conductivity, the discretizing errors increase with time, because the degree of particle irregularity increases with time due to particles moving with groundwater flow. If an initial particle distribution is evenly spaced, at an early time, the particle distribution is less irregular, and the smoothing error is dominant over discretizing error. With time increasing, the discretizing error increases, because the particle distribution becomes more and more irregular due to nonuniform flow in a heterogeneous field of hydraulic conductivity. Therefore, while SPH, C-SPH, and IC-SPH solutions of ADE may be similar in an early time, IC-SPH outperforms SPH and C-SPH when time increases. This is illustrated in the numerical examples presented in Section 3.2.

3. Numerical Investigations

To evaluate to what extent IC-SPH improves SPH and C-SPH solutions, two numerical experiments are conducted. The first numerical experiment is based on diffusion of a Gaussian contaminant plume with zero seepage velocity in a two-dimensional domain for which an analytical solution exists (Alvarado-Rodríguez et al., 2019; Beaudoin et al., 2003; Herrera & Beckie, 2013). The analytical solution is used to verify the numerical codes that implement SPH, C-SPH, IC-SPH, and to evaluate performance of IC-SPH for irregularly distributed particles. The second experiment considers an advection-dispersion problem in a domain with heterogeneous hydraulic conductivity. Since the second numerical experiment does not have an analytical solution, a reference solution of this example is obtained numerically by using a large number of irregularly distributed particles. To quantify the degree of irregular particle distributions in the two cases, the unity index, Q, is used. For particle i, its unity index is defined as (Zhu et al., 2015)

$$Q_i = \sum_j^{N_b} \frac{m_j}{\rho_j} W_{ij} \tag{30}$$

which, according to Equation 3, is the SPH approximation of a constant $C_i = 1$. For particle i with a complete support domain that is not intercepted by a boundary of the simulation domain, if the support domain has sufficient evenly spaced neighbor particles, then Q_i equals 1; otherwise, Q_i varies between particles and its histogram

has a peak around 1 (Zhu et al., 2015). After Q_i is evaluated for all the particles, the standard deviation of Q_i is estimated and used to quantify the degree of particle irregularity. A higher standard deviation indicates a higher degree of particle irregularity.

3.1. Diffusion Transport With Irregular Particle Distributions

3.1.1. Model Setup and Initial Particle Distribution

This numerical case considers a diffusive transport problem with zero seepage velocity in a two-dimensional square domain with the size of 60 × 60 m. The initial condition of the diffusive transport has an instantaneous Gaussian plume. The center of the Gaussian plume with the maximum concentration (C_0) is placed at location (x_0, y_0). For the two-dimensional diffusion problem with isotropic diffusion coefficient, the analytical solution of the normalized solute concentration (C/C_0) is (Alvarado-Rodríguez et al., 2019; Herrera & Beckie, 2013; Zimmermann et al., 2001)

$$\frac{C(x,t)}{C_0} = \frac{w^2}{(2tD + w^2)} \exp\left(\frac{-(x-x_0)^2 - (y-y_0)^2}{2(2tD + w^2)}\right) \tag{31}$$

where the components of molecular diffusion coefficient are set as $D = D_{xx} = D_{yy} = 1 \times 10^{-6}$ m^2/s. At $t = 0$, the initial plume is

$$\frac{C(x,t)}{C_0} = \exp\left(\frac{-(x-x_0)^2 - (y-y_0)^2}{2w^2}\right) \tag{32}$$

where $w = 2$ m controls the width of the Gaussian plume, and the plume center (x_0, y_0) is at the coordinates (30 m, 30 m). The analytical solution is used to compare performance of SPH, C-SPH, and IC-SPH with evenly spaced particles, irregularly distributed, and randomly distributed particles. For the SPH, C-SPH, and IC-SPH simulations, the total simulation time is set as $t = 10{,}000\Delta t = 1{,}000$ hr with the uniform time step of $\Delta t = 360$ s. This time step satisfies the relation of $\Delta t \le \varepsilon h^2/(D_{xx} + D_{yy})$ that has been used in literature (Alvarado-Rodríguez et al., 2019; Herrera & Beckie, 2013; Herrera et al., 2009), where $\varepsilon = 0.01$ is an empirical coefficient used in this study. Previous studies reported that $\varepsilon = 0.1$ is a good choice for SPH solutions (Alvarado-Rodríguez et al., 2019; Herrera & Beckie, 2013; Herrera et al., 2009). This study uses a small-time step because a highly irregular particle distribution is considered in the numerical experiments of this study. Using a small-time step helps capture spatial variation of solute concentrations for the irregular particle distribution. To be consistent, for all particle irregular distributions in the diffusive transport experiment, we use the same ε value of 0.01.

An irregular particle distribution is generated by adding a normally distributed perturbation with standard deviation σ to the evenly spaced particle position of spacing Δx. Particles are positioned in the domain size of [5 m, 55 m], Figure S1 in Supporting Information S1 shows the irregular particle distribution for $\sigma = \Delta x = \Delta y = 1$ m as an example. In this case, the particle spacing is of $\Delta x = \Delta y = 0.125$ m. Since groundwater velocity is zero in this numerical case, particles do not move. To study the effects of the different levels of particle irregularity on accuracy of SPH, C-SPH, and IC-SPH methods, a series of irregular particle configurations with different standard deviation values of $\sigma = 0$, $0.25\Delta x$, $0.5\Delta x$, and Δx and a random particle distribution are considered. The standard deviations of unity index for the five particle distributions are 0.0123, 0.0474, 0.0718, 0.0911, and 0.0963, respectively. As expected, the particle irregularity increases with the increase of the σ value. Zhu et al. (2015) stated, when the standard deviation of Q for a random particle distribution is close to 0.1, then the distribution is considered to be highly irregular. Therefore, the particle distributions for $\sigma = \Delta x$ and random particle distribution are highly irregular, because the standard deviations of Q for the two distributions equal 0.0911 and 0.0963, respectively.

3.1.2. Results for $\sigma = \Delta x$

Figure 2a plots concentration plumes of the analytical solution and numerical solutions of SPH, C-SPH, and IC-SPH. The SPH solution shown in Figure 2a2 substantially overestimates the maximum concentration at the plume center, where the overestimation is 0.0693, about 19% of the analytical solution maximum of 0.3571. This overestimation problem is alleviated in the C-SPH and IC-SPH solutions, being 10% for C-SPH and 1%

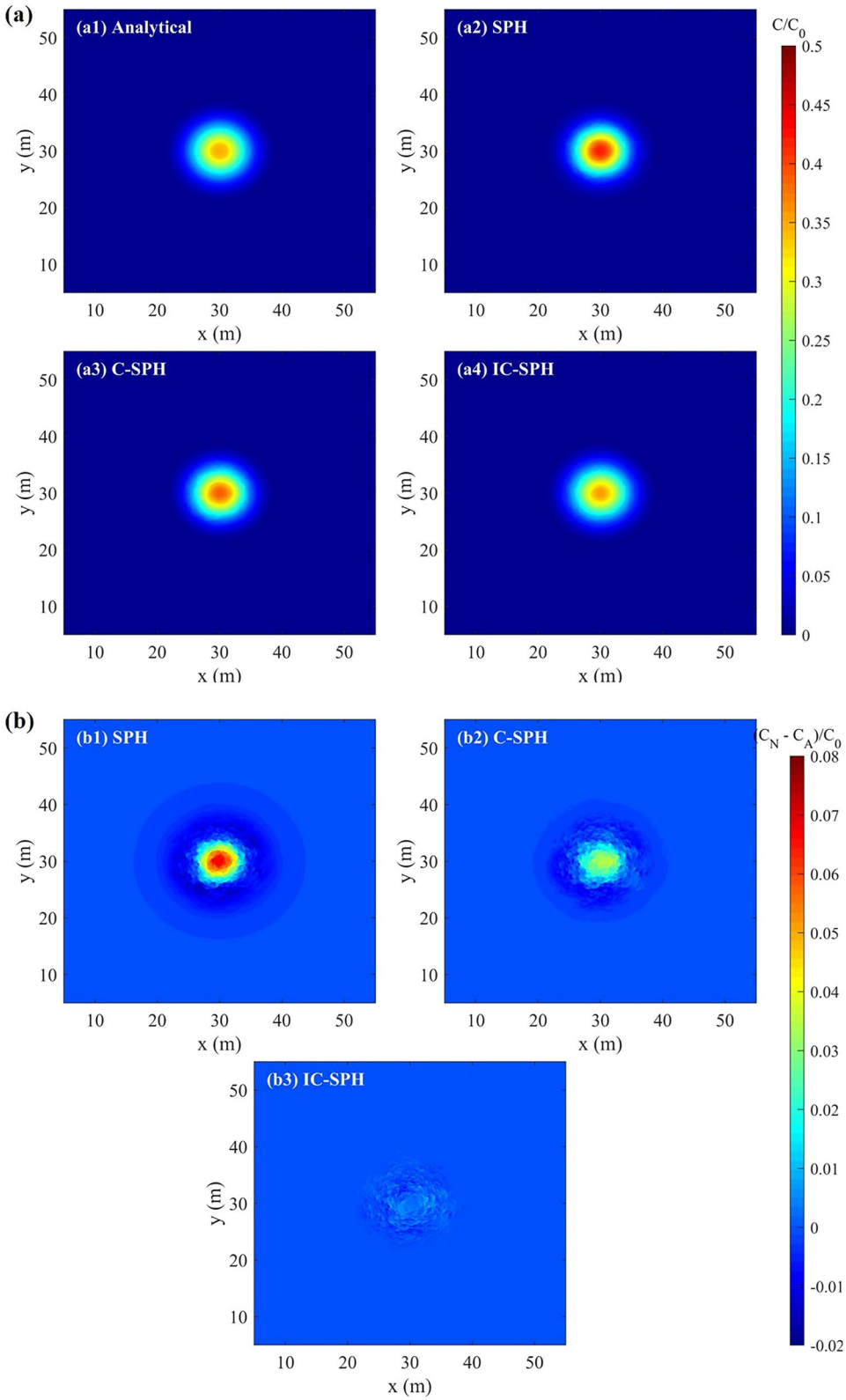
(a)
(a1) Analytical
(a2) SPH
(a3) C-SPH
(a4) IC-SPH
C/C0
0.5
0.45
0.4
0.35
0.3
0.25
0.2
0.15
0.1
0.05
0
y (m)
x (m)
(b)
(b1) SPH
(b2) C-SPH
(b3) IC-SPH
(CN - CA)/C0
0.08
0.07
0.06
0.05
0.04
0.03
0.02
0.01
0
-0.01
-0.02

Figure 2.

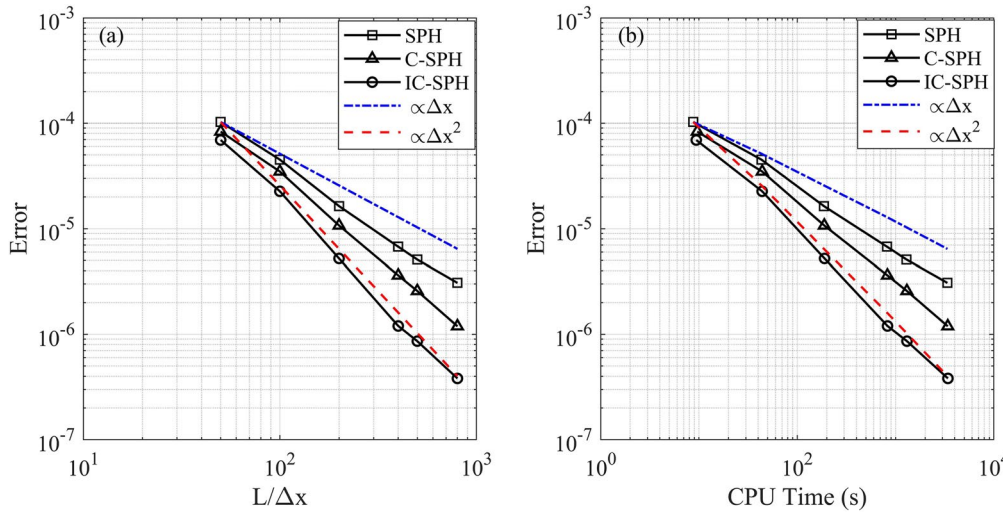

Figure 3. Error for normalized concentration (C/C_0) computed at simulation time t = 1,000 hr for SPH, Corrected Smoothed Particle Hydrodynamics (C-SPH), and Interactively Corrected Smoothed Particle Hydrodynamics (IC-SPH) numerical solutions (a) as a function of $L/\Delta x$ and (b) a function of CPU time (s) with an irregular particle distribution ($\sigma = \Delta x$) in the diffusive transport experiment. The irregular particle distribution is generated by adding random perturbations to evenly spaced particles; the perturbations follow a normal distribution with the mean of zero and the standard deviation of σ.

for IC-SPH. The IC-SPH solution is visually more accurate than the C-SPH solution, which in turn is better than the SPH solution. This is also observed in Figure 2b, which plots plumes of concentration differences between the three numerical solutions and the analytical solution for the simulation with $\sigma = \Delta x$ at the end of simulation time t = 1,000 hr. As shown in Figures 2b2 and 2b3, in the vicinity of the plume center (where the maximum concentration occurs), the differences between the IC-SPH and analytical solutions are smaller than those between the C-SPH and analytical solutions, indicating that IC-SPH outperforms C-SPH, although the outperformance is marginal for Figure 2b.

Figure 3a plots the numerical error (relative to the analytical solution) as a function of $L/\Delta x$ for the three numerical solutions with $\sigma = \Delta x$, to examine convergence of the numerical solutions to the analytical solution. The error is defined as Error = $\|C_N/C_0 - C_A/C_0\|_2/N$, where C_N/C_0 is the numerical solution given by SPH, C-SPH, or IC-SPH, C_A/C_0 is the analytical solution, and N is the total number of particles. This error metric is slightly different from the L^2 norm as it is divided by particle number N, and the metric was also used by Herrera et al. (2009) and Avesani et al. (2015). Based on the error, convergence rate of the numerical solutions is evaluated as $\log\left(\frac{error_{\Delta x_2}}{error_{\Delta x_1}}\right)/\log\left(\frac{\Delta x_2}{\Delta x_1}\right)$ for six Δx values ranging between Δx = 1 m ($\Delta x/L = 0.02$) and $\Delta x = 0.0625$ m ($\Delta x/L = 0.00125$). Using the middle Δx values, the convergence rate is 1.279, 1.566, and 2.120 for SPH, C-SPH, and IC-SPH, respectively. The convergence rate is the largest for IC-SPH, indicating that IC-SPH outperforms SPH and C-SPH in terms of convergence. The convergence rate is also estimated for two cases of anisotropic dispersion, i.e., (a) $D_{yy} = 0.1D_{xx} = 1 \times 10^{-7}$ m^2/s and $D_{xy} = 0$ and (b) $D_{xx} = 0.775 \times 10^{-6}$ m^2/s, $D_{yy} = 0.325 \times 10^{-6}$ m^2/s, and $D_{xy} = 0.433 \times 10^{-6}$ m^2/s with $h = 2.5\Delta x$ and $\Delta x = 0.125$ m. The results are shown in Figure S2 in Supporting Information S1. The figure indicates that IC-SPH has the largest convergence rate, suggesting that the IC-SPH solutions are more accurate than the SPH and C-SPH solutions for the two problems with anisotropic dispersion.

Figure 3b plots the errors with the CPU times for the six Δx values ranging between Δx = 1 m ($\Delta x/L = 0.02$) and $\Delta x = 0.0625$ m ($\Delta x/L = 0.00125$), and the CPU time is for a computer with Intel(R) Core (TM) i7-8550U CPU of 1.99 GHz. Table 1 lists the errors and the CPU time for the six Δx values. Figure 3b does not visually show

Figure 2. (a) Concentration plumes of (a1) analytical solution, (a2) Smoothed Particle Hydrodynamics (SPH) solution, (a3) Corrected Smoothed Particle Hydrodynamics (C-SPH) solution, and (a4) Interactively Corrected Smoothed Particle Hydrodynamics (IC-SPH) solution of normalized concentration (C/C_0) at simulation time t = 1,000 hr for an irregular particle distribution of the diffusive transport experiment. (b) Plumes of concentration differences between normalized numerical solution, (C_N/C_0), and normalized analytical solution, (C_A/C_0), for (b1) SPH, (b2) C-SPH, and (b3) IC-SPH of the diffusive transport experiment. A total of 160,801 particles ($h = 1.5\Delta x$ and $\Delta x = 0.125$ m) are used for the simulation.

Table 1
Convergence Tests for the Diffusive Transport Experiment of SPH, C-SPH, and IC-SPH Solutions With the Irregular Particle Distribution of $\sigma = \Delta x$

	Number of particles (N)	$\Delta x/L$	Error	O(Error)	CPU time (s)
SPH	2,601	0.02	1.028E−04	1.187	8.73
	10,201	0.01	4.516E−05	1.465	43.23
	40,401	0.005	1.636E−05	1.279	186.9
	160,801	0.0025	6.739E−06	1.254	819.02
	251,001	0.002	5.095E−06	1.074	1293.58
	641,601	0.00125	3.075E−06	—	3369.93
C-SPH	2,601	0.02	8.340E−05	1.261	9.61
	10,201	0.01	3.481E−05	1.701	44.01
	40,401	0.005	1.071E−05	1.566	188.48
	160,801	0.0025	3.616E−06	1.518	827.15
	251,001	0.002	2.577E−06	1.639	1303.39
	641,601	0.00125	1.193E−06	—	3397.42
IC-SPH	2,601	0.02	6.930E−05	2.116	9.39
	10,201	0.01	2.261E−05	2.120	43.95
	40,401	0.005	5.215E−06	2.120	189.57
	160,801	0.0025	1.200E−06	1.488	828.06
	251,001	0.002	8.609E−07	1.731	1306.31
	641,601	0.00125	3.816E−07	—	3409.74

difference of CPU time between SPH, C-SPH, and IC-SPH, and Table 1 indicates that the CPU time of IC-SPH is only slightly larger than those of SPH and C-SPH. For example, the CPU time for 160,801 particles is 819.02, 827.15, and 828.06 for SPH, C-SPH, and IC-SPH, respectively. The similarity in the CPU times of the three solutions is attributed to the fact that, for the diffusive transport experiment, IC-SPH only needs to search for neighbor particles once. This is not the case for the advection-dispersion problem in which particles move with groundwater flow, and the CPU time of IC-SPH is significantly larger than those of SPH and C-SPH, as shown in Section 3.2.2.

3.1.3. Results for Different Levels of Particle Irregularity

Figure 4 plots the analytical and numerical solutions at simulation time $t = 1{,}000$ hr along the cross-section of $y = 30$ m obtained using four irregular particle distributions (generated using the σ values of 0, $0.25\Delta x$, $0.5\Delta x$, and Δx) and one random particle distribution (generated using the MATLAB *Rand* function). Since there are no particles exactly located at the line of $y = 30$ m for irregular and random particle distributions, we selected the particles within the range of $y = 29.98$ m and $y = 30.02$ m to compare the three numerical solutions with the analytical solution. To avoid sampling error, we used one-dimensional diffusive transport problem with 1,001 particles which are irregularly distributed in the line with domain size of [5 m, 55 m]. The profiles of the analytical and the three numerical solutions are shown in Figure S3 in Supporting Information S1.

For the diffusive transport problem, Figure 4a shows that, for $\sigma = 0$ with the evenly spaced particle distribution, the numerical solutions are visually identical to the analytical solution. Figures 4b–4d show that, when σ increases (i.e., the particle distribution becomes more irregular), the SPH and C-SPH solutions increasingly deviate from the analytical solution, and the SPH solution is always less accurate than the C-SPH solution, especially in the maximum concentration locations. It is also the case for Figure 4e with the randomly generated particle distribution.

In IC-SPH, the over-diffused concentrations in Figures 4b and 4c and under-diffused concentrations in Figures 4d and 4e are due to different particle irregularities and selection of smoothing lengths. Increasing the smoothing length leads to more accurate solutions. In SPH, the first-order derivatives of concentration in space are usually underestimated, because the integrations of $(x_i - x_j)\,\nabla_{i,x} W_{ij}$ over the support domain are usually less than 1 (e.g., 0.6233 in Figure A1b) for a limited number of irregularly distributed particles. As a result, the time rate change of concentration in Equation 29 is underestimated, and this leads to the overestimation of the normalized concentration at the plume center and correspondingly underestimation away from the plume center (Figures 2 and 4). The problems of overestimation at the plume center and underestimation at locations away from the plume center are alleviated by C-SPH and IC-SPH because of using the corrected and interactively corrected kernel gradients, respectively. In addition, the IC-SPH solution with the interactively corrected kernel gradients is less sensitive to smoothing length h than the SPH solution is, as indicated in Figure S4 in Supporting Information S1 with different values of h.

3.2. Advection-Dispersion in a Nonuniform Velocity Field

This numerical experiment considers both advection and dispersion, and is thus more realistic than the first numerical experiment that considers diffusion only. The objective of this numerical experiment is to evaluate the performance of IC-SPH for simulating solute transport in a two-dimensional heterogeneous aquifer.

3.2.1. Model Setup

This numerical experiment considers solute transport in a two-dimensional, confined domain with the size of 40×15 m. A heterogeneous hydraulic conductivity field is generated by using the "gstat" geostatistical package (Pebesma, 2004). It is assumed that the natural logarithm of the hydraulic conductivity, $Y = \ln K$, follows the

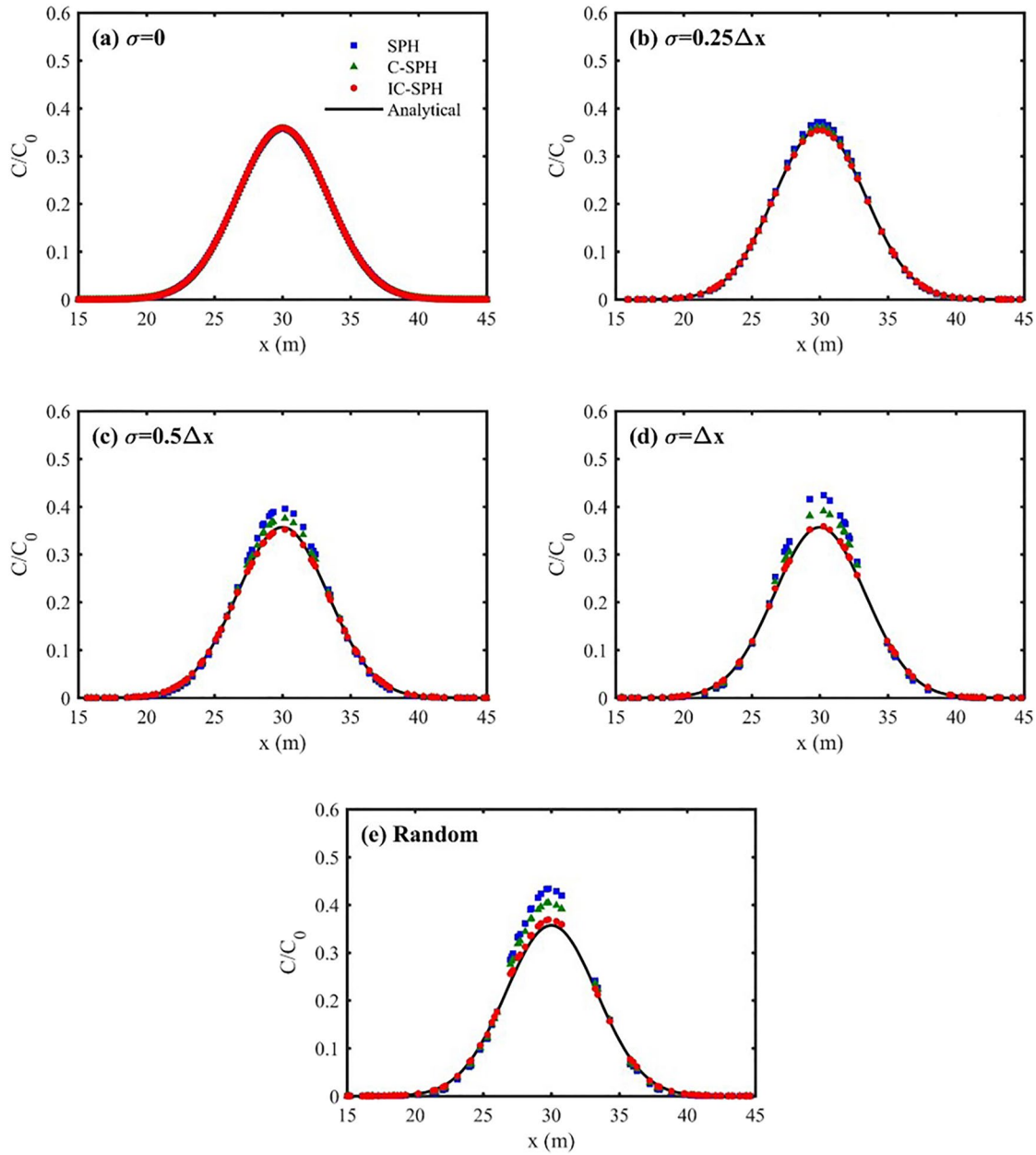

Figure 4. Profiles of the analytical, Smoothed Particle Hydrodynamics (SPH), Corrected Smoothed Particle Hydrodynamics (C-SPH), and Interactively Corrected Smoothed Particle Hydrodynamics (IC-SPH) solutions of normalized concentration (C/C_0) along the line of $y = 30$ m at simulation time $t = 1{,}000$ hr in the numerical experiment of diffusive transport. The particle distributions are generated using a Gaussian perturbation with the mean of zero and the standard deviation of (a) $\sigma = 0$, (b) $\sigma = 0.25\Delta x$, (c) $\sigma = 0.5\Delta x$, and (d) $\sigma = \Delta x$ with $\Delta x = 0.125$ m and $h = 1.5\Delta x$ ($N = 160{,}801$).

normal distribution with mean of $<Y> = 1$ and variance of $\sigma_Y^2 = 1$. An exponential covariance function with the correlation length of $IY = 1$ m is used to generate the heterogeneous hydraulic conductivity field. Figure 5 shows the generated K field. The flow direction is from a constant-head boundary at the left side to the constant-head boundary at the right side of the simulation domain; the top and bottom boundaries are set as no-flow boundaries. The groundwater flow is assumed to be steady, and MODFLOW 2000 (Harbaugh, 2000) is used to solve the flow problem with a uniform block size of 0.125×0.125 m. Seepage velocity is evaluated by using a constant porosity of 0.3 over the simulation domain. The velocity field is also shown in Figure 5.

The resulting velocity field from MODFLOW is used to simulate solute transport. The initial condition of the advection-dispersion problem has an instantaneous concentration C_0 that is a constant over a square with the size

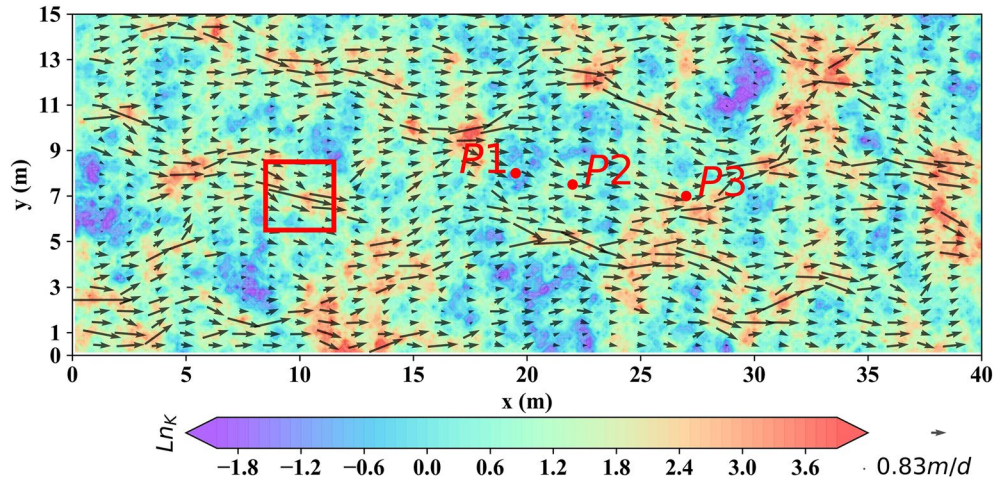

Figure 5. Groundwater seepage velocity field for a heterogeneous field of hydraulic conductivity with $\sigma_Y^2 = 1$, with Y being log hydraulic conductivity. The arrows denote magnitude and direction of the seepage velocity. The red box represents the area of initial concentration domain. Points P1(19.5 m, 8 m), P2(22 m, 7.5 m), and P3(27 m, 7 m) are three locations where breakthrough curves are generated.

of $L = 3$ m centered at the location of (10 m, 7 m). The contaminant source area and three observation points P1, P2, and P3 are shown in Figure 5. Initial particles are evenly placed at the domain with the spatial resolution of $\Delta x = \Delta y = 0.0625$ m, and this results in a total of $N = 76{,}800$ particles. The kernel smoothing length is set as $h = 2\Delta x = 0.125$ m. The dispersion coefficient is isotropic with $D = D_{xx} = D_{yy} = 1 \times 10^{-7}$ m^2/s. The total simulation time is set as $t = 1{,}200\Delta t$ with a uniform time step of $\Delta t = 1{,}800$ s estimated using an empirical ε value of 0.02. Table 2 lists the parameter values used to solve the flow and solute transport model.

In addition to $\sigma_Y^2 = 1$, we also use $\sigma_Y^2 = 0.2$ and 0.5 to generate two additional fields of heterogeneous hydraulic conductivity for evaluating the performance of SPH, C-SPH, and IC-SPH with different levels of particle irregularity. The standard deviation of unity index Q for the three σ_Y^2 values are shown in Figure 6 with different simulation times. As expected, for each σ_Y^2 value, the irregularity of the particle distributions increases with time due to particle movement. When σ_Y^2 increases, heterogeneity of hydraulic conductivity increases, and irregularity of the particle distributions increases accordingly. Figure 6 shows that particle irregularity increases and then stabilizes, which is consistent with the study of Monaghan (2005) that particles become ordered after a period of time of groundwater flow.

Table 2
Parameter Values Used in Groundwater Flow and Solute Transport Modeling of the Advection-Dispersion Experiment

Description	Value
Variance of ln(K)	1
Correlation length of ln(K) (I_Y)	1 m
Domain dimension	40 × 15 m
Grid size in flow field (Δ)	0.125 m
Mean velocity in x (v_x)	0.83 m/day
Max. velocity in x (v_{max})	4.12 m/day
Initial plume size	3 × 3 m
Initial plume center	(10 m, 7 m)
Peclet number ($v_x I_Y/D$)	96
Mean CFL number ($v_x \Delta t/\Delta$)	0.28

Since there is no analytical solution for this numerical experiment, to evaluate the performance of SPH, C-SPH, and IC-SPH, a numerical solution given by SPH is used as the reference solution. The reference SPH solution is expected to be accurate by using a fine particle spacing of $\Delta x = \Delta y = 0.02$ m ($N = 750{,}000$) and adequate smoothing length of $h = 0.3$ m. These values are chosen based on the general principles discussed in Section 2.4 that accurate SPH solutions can be obtained by using an adequate value of smoothing length, h, to ensure a large number of particles within a support domain (Herrera et al., 2009; Zhu et al., 2015). The specific reasons for the setting of the reference solution are explained using Figures B1 and B2 in Appendix B. Since the particles used for the three numerical solutions ($N = 76{,}800$) are different from the particles used for the reference solution ($N = 750{,}000$), to compare the SPH, C-SPH, and IC-SPH solutions with the reference solution, the four solutions are interpolated to a grid with the uniform size of $\Delta x = \Delta y = 0.1$ m. The interpolation is conducted by using the MATLAB scatter interpolation function, *ScatteredInterpolant*, with the "*natural*" option of the function to facilitate the comparison between the numerical solutions and the reference solution. The natural neighbor interpolation is a

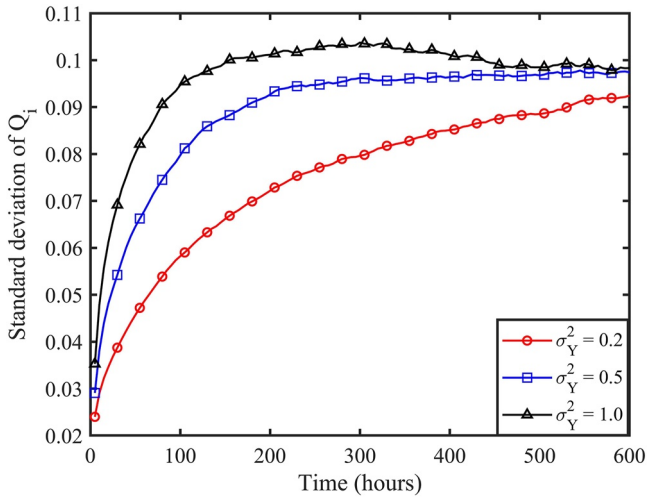

Figure 6. Variation of the standard deviation of unity index, Q_i, as a function of time for three fields of heterogeneous hydraulic conductivity with different σ_Y^2 values.

weighted average method. The weights are area-based to compensate for data density variation, and are superior to distance-based weights. As a result, the *ScatteredInterpolant* function is a robust scatter point interpolation method, and performs well in areas of both clustered and sparse data points. The interpolation error is not expected to affect the conclusions of this study.

3.2.2. Results

Figure 7 shows the evolution of particle distributions (the first row) and the simulated plumes by SPH (the second row), C-SPH (the third row), and IC-SPH (the last row) methods for the heterogeneous field of hydraulic conductivity generated with $\sigma_Y^2 = 1$. The three columns of Figure 7 are for the results at simulation times of $t = 100$, 300, and 500 hr Figures 7a1–7cl only plots the particles whose normalized concentration (C/C_0) larger than the threshold of 10^{-4}. The three plots show that there are more (less) particles in the areas where pathlines converge (diverge) as indicated by the velocity field shown in Figure 7. This spatial pattern was also observed by Tartakovsky (2010). For the simulated concentration, the SPH, C-SPH, and IC-SPH solutions at $t = 100$ hr are visually similar, as shown in Figures 7a2-7a4. When time increases, the particle distribution becomes more and more irregular (Figures 7b1 and 7c1), and the SPH, C-SPH, and IC-SPH solutions become visually different. The CPU times for SPH, C-SPH, and IC-SPH numerical solutions are 791.9.1, 2396.49, and 4532.99 s, respectively. The

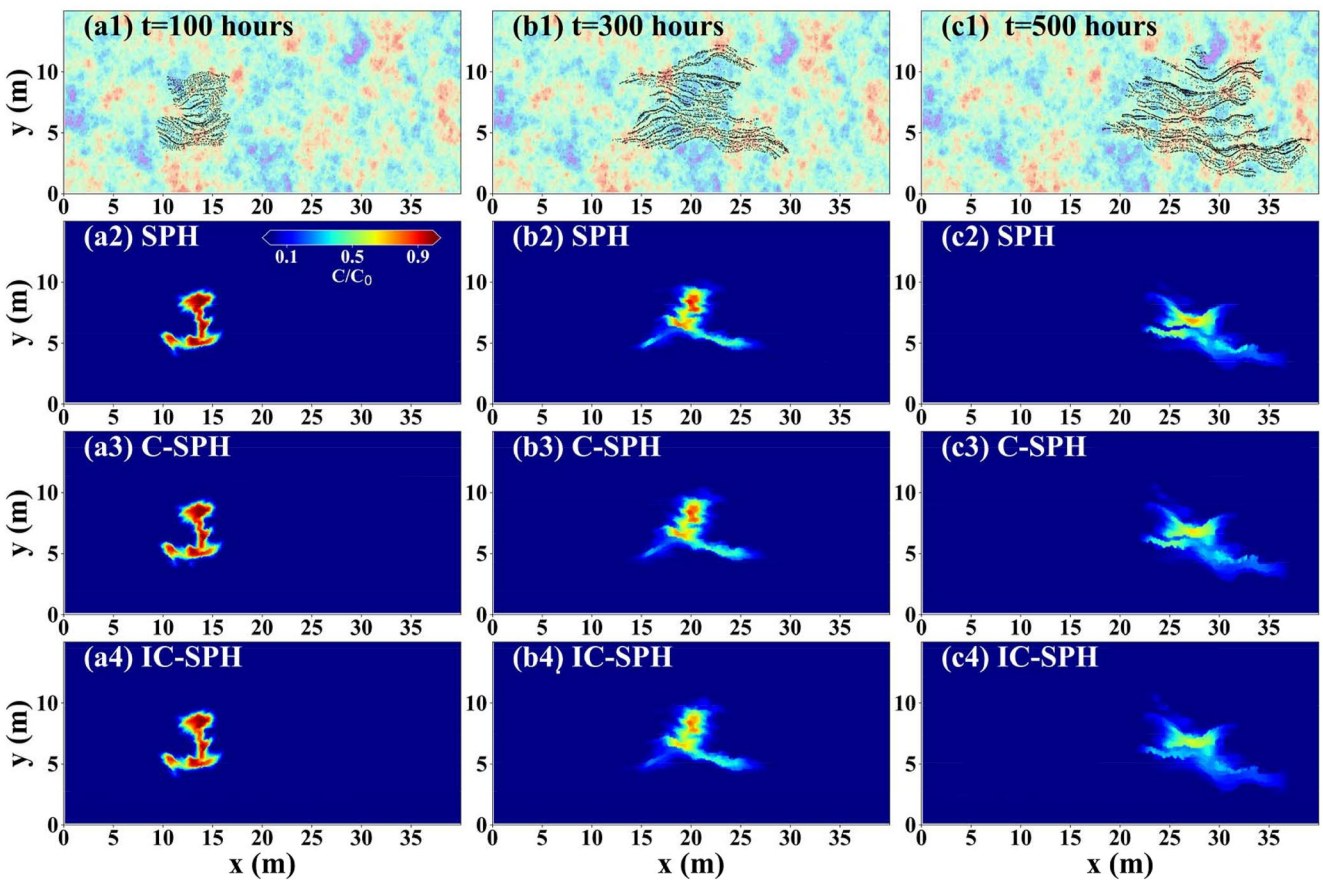

Figure 7. (a1) Particle distribution, (a2) Smoothed Particle Hydrodynamics (SPH) solution, (a3) Corrected Smoothed Particle Hydrodynamics (C-SPH) solution, and (a4) Interactively Corrected Smoothed Particle Hydrodynamics (IC-SPH) solution for simulation time $t = 100$ hr (b1–b4) are for $t = 300$ hr, and (c1–c4) are for $t = 500$ hr. Only particles whose normalized concentrations are larger than the threshold of 10^{-4} are shown.

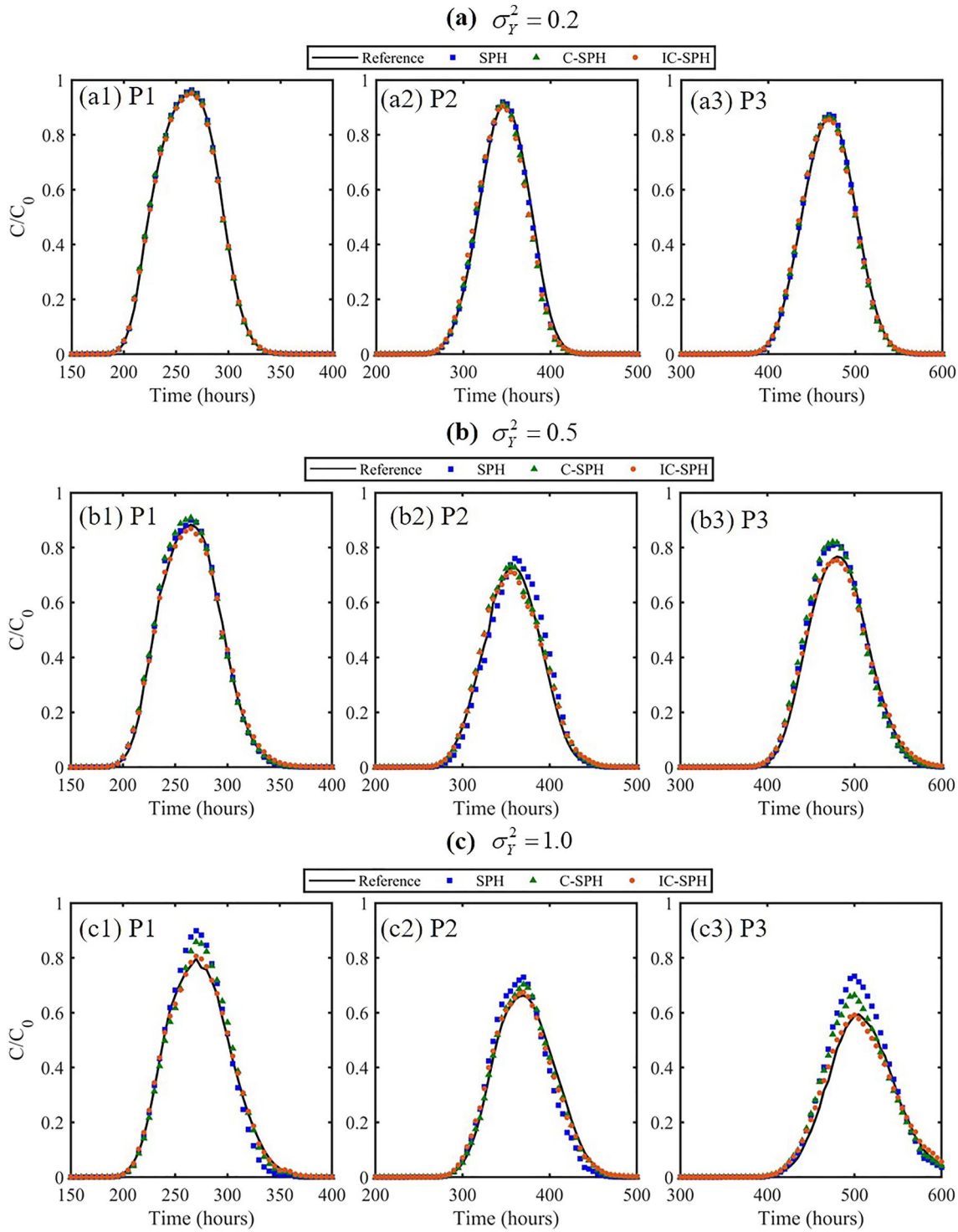

Figure 8. Breakthrough curves of normalized concentration (C/C_0) at points P1, P2, and P3 shown in Figure 5 for heterogeneous fields of hydraulic conductivity generated with (a1)–(a3) $\sigma_Y^2 = 0.2$, (b1)–(b3) $\sigma_Y^2 = 0.5$, and (c1)–(c3) $\sigma_Y^2 = 1.0$.

CPU time of IC-SPH is about six times as many as that of SPH, because IC-SPH needs to search neighbor particles and to modify kernel gradients for the particles at every time step when particle locations change with time.

To better evaluate the SPH, C-SPH, and IC-SPH solutions, Figure 8 plots the breakthrough curves at the three points of P1, P2, and P3 for the three σ_Y^2 values of $\sigma_Y^2 = 0.2, \sigma_Y^2 = 0.5$, and $\sigma_Y^2 = 1.0$. For $\sigma_Y^2 = 0.2$, Figures 8a1–8a3

show that the three numerical solutions are all close to the reference solution. The reason is that, for the small σ_Y^2 value, the particle distribution is relatively regular, and the discretizing error caused by irregular particle distributions is small and cumulative discretizing error caused by irregular particle distribution is small with small change of concentration. When σ_Y^2 increases to 0.5 and 1, SPH and C-SPH solutions become less accurate, since particle irregularity increases with the heterogeneity of hydraulic conductivity field. The IC-SPH solution is more accurate than the SPH and C-SPH solutions at all the three points and for all the three σ_Y^2 values, indicating that IC-SPH outperforms SPH and C-SPH. It is also noted that the difference between SPH and IC-SPH solutions increases with the increasing of hydraulic conductivity heterogeneity. This is not surprising, because heterogeneous hydraulic conductivity is a factor that causes particle irregularity, as shown in Figure 6. Figures 8c1–8c3 show that SPH and C-SPH perform better at point P2 than at points P1 and P3. This is attributed to the less nonuniform velocity at point P2 than at points P1 and P3. Figure 5 shows that velocity magnitude and direction are similar around point P2 but have more variation around points P1 and P3. The breakthrough curves at the three points for anisotropic dispersion coefficients are shown in Figure S5 in Supporting Information S1. For the anisotropic problem, a further study is needed to resolve the issue of negative concentrations, which, however, is beyond the scale of this study.

4. Conclusions

This study develops the IC-SPH method for improving SPH solutions of groundwater solute transport in a nonuniform velocity field where a particle distribution becomes irregular due to particle movement with flow. For irregularly distributed particles, SPH cannot yield accurate solutions of ADE, because the antisymmetric property may not be satisfied. IC-SPH is similar to C-SPH in nature, in that both methods make correction to kernel gradients. While the correction of C-SPH for particle i is based on particle j within the support domain of particle i, the correction of IC-SPH is an interactive correction to further use the particles in the support domain of particle j. The interactive correction alleviates accumulation of discretizing errors, and thus makes IC-SPH solutions more accurate than those of C-SPH.

Numerical solutions of SPH, C-SPH, and IC-SPH are evaluated in two numerical examples involving diffusion and advection-dispersion problems. In comparison with the reference solutions (analytical for the first experiment and numerical for the second experiment), IC-SPH gives most accurate ADE solutions for highly irregular particle distributions, and has the largest convergence rate to the analytical solution. It is especially the case for the locations with maximum solute concentrations (Section 3.1.2) and/or with more nonuniform flow velocity (Section 3.2.2). It is also the case for late simulation times when particle distributions become more irregular than at early simulation times. It, however, should be noted that the computational cost of IC-SPH is substantially larger than that of SPH and C-SPH, because IC-SPH requires constructing extra matrices and solving more systems of equations for correcting the kernel gradients.

This study is focused on the advection-dispersion equation with isotropic dispersion coefficients. While the Supporting Information has a discussion on certain results for anisotropic dispersion coefficients, the problem of negative concentrations occurring with anisotropic dispersion coefficient is not tackled in this study. This problem may be caused not only by intrinsic deficiencies of SPH but also by the parabolic character of the classical advection-dispersion equation (Alvarado-Rodríguez et al., 2019). It will be explored in a future study whether IC-SPH can help address the problem of negative concentrations with anisotropic dispersion coefficients.

Appendix A: Fundamental of SPH Methods and Particle Irregularity Problems

The approximations of concentration $C(\mathbf{x})$ and its first spatial derivative $\nabla C(\mathbf{x})$ at position $\mathbf{x}$ can be written as (Monaghan, 2005)

$$\langle C(\mathbf{x})\rangle = \int_\Omega C(\mathbf{x}')\, W(\mathbf{x}-\mathbf{x}', h)\, d\mathbf{x}' \tag{A1}$$

$$\langle \nabla C(\mathbf{x})\rangle = -\int_\Omega C(\mathbf{x}')\, \nabla W(\mathbf{x}-\mathbf{x}', h)\, d\mathbf{x}' \tag{A2}$$

where $\langle\rangle$ denotes an approximation, Ω is the support domain, W is a kernel function, $\nabla W(\mathbf{x}-\mathbf{x}', h) = \nabla W(\mathbf{x}-\mathbf{x}', h)|_{\mathbf{x}'}$, and h is the smoothing length that defines the support domain Ω of kernel function W. It should be noted that, while we use a compact support domain to improve computational efficiency in this study, noncompact support domains and kernels also work in SPH. $\mathbf{x}'$ is the location of neighbor particles within the support domain of interests of particle $\mathbf{x}$. The information of the particle at location $\mathbf{x}$ is determined by the information of neighbor particles (Liu & Liu, 2003). The kernel function should be sufficiently smooth and satisfy the following properties: normalization condition, $\int_\Omega W(\mathbf{x}-\mathbf{x}', h)\, d\mathbf{x}' = 1$, symmetric property, $\int_\Omega (\mathbf{x}'-\mathbf{x}) W(\mathbf{x}-\mathbf{x}', h)\, d\mathbf{x}' = 0$, delta function property, $\lim_{h\to 0} W(\mathbf{x}-\mathbf{x}', h) = \delta(\mathbf{x}-\mathbf{x}')$, positive property, $W(\mathbf{x}-\mathbf{x}') \geq 0$, and monotonical property that W monotonically decreases with h (Liu & Liu, 2010). In this work, we choose the commonly used cubic B-spline (Avesani et al., 2015; Boso et al., 2013; Monaghan, 2005)

$$W = W_0 \times \begin{cases} 2/3 - q^2 + q^3/2 & 0 \leq q < 1 \\ (2-q)^3/6 & 1 \leq q < 2 \\ 0 & q \geq 2, \end{cases} \tag{A3}$$

where $q = |\mathbf{x}-\mathbf{x}'|/h$ is the relative distance between two particles at locations $\mathbf{x}$ and $\mathbf{x}'$, W_0 is a normalization factor with $W_0 = 1/h$ for a one-dimensional space, $W_0 = 15/\left(7\pi h^2\right)$ for a two-dimensional space and $W_0 = 3/\left(2\pi h^3\right)$ for a three-dimensional space.

The integral in Equations A1 and A2 around particle i within the particle's support domain can be discretized as a summation over all neighbor particles j. This gives the so-called particle approximation as follows:

$$\langle C(\mathbf{x}_i)\rangle = \sum_{j=1}^{N_b} \frac{m_j}{\rho_j} C(\mathbf{x}_j) W_{ij} \tag{A4}$$

$$\langle \nabla C(\mathbf{x}_i)\rangle = \sum_{j=1}^{N_b} \frac{m_j}{\rho_j} C(\mathbf{x}_j) \nabla_i W_{ij} \tag{A5}$$

where N_b is the number of particles within the support domain of the ith particle. $\mathbf{x}_i$ and $\mathbf{x}_j$ are the positions of particles i and j, respectively, $W_{ij} = W(|\mathbf{x}_i - \mathbf{x}_j|, h)$, $\nabla_i W_{ij} = -\nabla_j W_{ij}$ is the gradient of the kernel function at particle i, m_j and ρ_j are the mass and density of the jth particle, respectively. With $m_j/\rho_j = 1/n_j = V_j$, where V_j is the volume associated with particle j. The particle number density n_j is expressed as $n_j = \sum_k W(\mathbf{x}_j - \mathbf{x}_k, h)$ (Tartakovsky & Meakin, 2005), which means the number of particles per unit volume, where $\mathbf{x}_k$ is the location of neighbor particles of particle j.

It has been noted that, for constant $C(\mathbf{x}_i)$, the approximation of the derivative in Equation A5 is not necessarily zero, if the antisymmetric property of the first-order derivative of W, $\sum_{j=1}^{N_b} (m_j/\rho_j) \nabla_i W_{ij} = 0$, is not satisfied. This encourages other ways to derive the approximation of the derivatives of C (Liu & Liu, 2010; Monaghan, 2005). The antisymmetric form of the first-order derivative in space is given as

$$\langle \nabla C_i\rangle = \sum_{j}^{N_b} \frac{m_j}{\rho_j} (C_j - C_i) \nabla_i W_{ij} \tag{A6}$$

where $C_j = C(\mathbf{x}_j)$ and $C_i = C(\mathbf{x}_i)$. This equation is commonly used in SPH, since it improves particle approximation accuracy (Liu & Liu, 2006). For this reason, this study uses Equation A6 rather than Equation A5.

To have an accurate particle approximation of the first-order derivatives of concentration in Equation A6, the first-order derivatives of the kernel need to satisfy the so-called antisymmetric property (bib_Chen_and_Beraum_2000Chen & Beraum, 2000). To illustrate this, we apply the Taylor series expansion to $C_j = C(\mathbf{x}_j)$ at particle location $\mathbf{x}_i = \{x_i, y_i, z_i\}$, and retain the first-order derivatives, i.e.,

$$C_j \approx C_i + \left(\mathbf{x}_j^\alpha - \mathbf{x}_i^\alpha\right) \frac{\partial C_i}{\partial \mathbf{x}_i^\alpha} = C_i + (x_j - x_i) \frac{\partial C_i}{\partial x_i} + (y_j - y_i) \frac{\partial C_i}{\partial y_i} + (z_j - z_i) \frac{\partial C_i}{\partial z_i} \tag{A7}$$

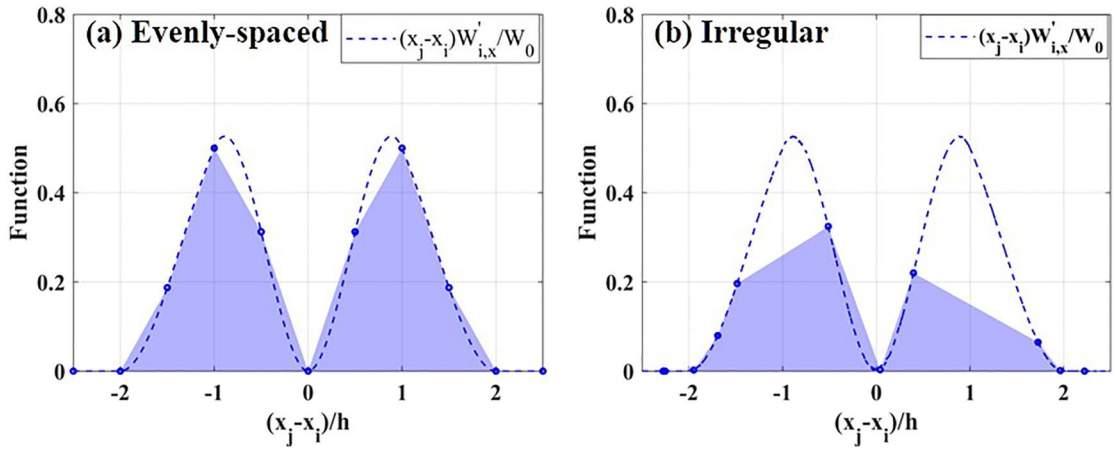

Figure A1. Illustration for antisymmetric property of Smoothed Particle Hydrodynamics (SPH) kernel gradients with (a) evenly spaced and (b) irregularly distributed particles in a one-dimensional domain.

Taking the first-order derivatives of C_i in the x direction as an example, based on Equation A6 of the derivative and Equation A7 of the Taylor series expansion of C_j, we have

$$\left\langle \frac{\partial C_i}{\partial x_i} \right\rangle = \sum_{j=1}^{N_b} \frac{m_j}{\rho_j} (C_j - C_i) \frac{\partial W_{ij}}{\partial x_i} \approx \frac{\partial C_i}{\partial x_i} \sum_{j=1}^{N_b} \frac{m_j}{\rho_j} x_{ji} \frac{\partial W_{ij}}{\partial x_i} + \frac{\partial C_i}{\partial y_i} \sum_{j=1}^{N_b} \frac{m_j}{\rho_j} y_{ji} \frac{\partial W_{ij}}{\partial x_i} + \frac{\partial C_i}{\partial z_i} \sum_{j=1}^{N_b} \frac{m_j}{\rho_j} z_{ji} \frac{\partial W_{ij}}{\partial x_i} \tag{A8}$$

where $x_{ji} = x_j - x_i$, $y_{ji} = y_j - y_i$, and $z_{ji} = z_j - z_i$. The antisymmetric property for the first-order derivative of the kernel in the x direction is as follows: $\sum_{j=1}^{N_b} \frac{m_j}{\rho_j} x_{ji} \frac{\partial W_{ij}}{\partial x_i} = 1$, $\sum_{j=1}^{N_b} \frac{m_j}{\rho_j} y_{ji} \frac{\partial W_{ij}}{\partial x_i} = 0$, and $\sum_{j=1}^{N_b} \frac{m_j}{\rho_j} z_{ji} \frac{\partial W_{ij}}{\partial x_i} = 0$. If the three equations are satisfied, then $\left\langle \frac{\partial C_i}{\partial x_i} \right\rangle \approx \frac{\partial C(\mathbf{x}_i)}{\partial x_i}$ with a second-order accuracy in terms of $r = |\mathbf{x}_j - \mathbf{x}_i|$, where r is the distance between particles i and j (Liu & Liu, 2010).

The antisymmetric property may not be satisfied for irregularly distributed particle, and this is demonstrated in Figure A1 for evenly spaced and irregular particle distributions in a one-dimensional domain. For the evenly spaced particle distribution, any two neighbor particles have the same distance of $\Delta x = 0.125$ m. The kernel function defined in Equation 5 is used for Figure 1, with $h = 2\Delta x$ and the radius of the support domain Ω as $2h = 4\Delta x$. Figure A1a shows function $(x_j - x_i) W'_{i,x}/W_0$ as a function of $(x_j - x_i)/h$ for a number of evenly spaced particles; Figure A1b is similar to Figure A1a but for irregularly distributed particles. The irregular particle distribution is generated by adding a normally distributed perturbation with standard deviation of $\sigma = \Delta x$ to the evenly spaced particle positions. For this one-dimensional problem, we only examine whether $\sum_{j=1}^{N_b} \frac{m_j}{\rho_j} x_{ji} \frac{\partial W_{ij}}{\partial x_i} = 1$ is satisfied, i.e., whether the areas in blue in Figures A1a and A1b equal 1. For Figure A1a with the evenly spaced particles, $\sum_{j=1}^{N_b} \frac{m_j}{\rho_j} x_{ji} \frac{\partial W_{ij}}{\partial x_i} = 0.9999$, which is close to 1. For Figure A1b with the irregularly distributed particles, this term becomes 0.6233, indicating that the antisymmetric property is not satisfied. The two figures demonstrate that, for irregularly distributed particles, the SPH-based approximations of the first-order derivatives of concentration may not be accurate.

Appendix B: Reference Solutions of the Advection-Dispersion Transport Experiment

A large number of neighbor particles are needed for obtaining an accurate reference solution using a standard SPH method for the advection-dispersion problem with a nonuniform velocity field. Accuracy of SPH solutions depends on not only particle spacing but also the number of neighbor particles within a support domain whose size is defined by smoothing length h. The reason is that the SPH solution error due to SPH approximation of integral by summation depends on N_b (the number of neighbor particles), not N (the total number of particles), when particles are redistributed by a nonuniform flow (Zhu et al., 2015). Increasing N may result in

limited improvement on accuracy of SPH solutions. For the advection-dispersion problem with heterogeneous fields of hydraulic conductivity, particles moving with nonuniform velocity leads to more (less) particles in areas where pathlines converge (diverge). While increasing particle number, N, increases the number of particles in a pathline-converging area, it does not necessarily increase the number of particles in a pathline-diverging area. As a result, using more particles does not necessarily improve SPH solution accuracy. This is illustrated in Figure B1 with the particle spacing decreasing from $\Delta x = 0.03125$ m ($N = 307{,}200$) to $\Delta x = 0.02$ m ($N = 750{,}000$) and further to $\Delta x = 0.0125$ m ($N = 1{,}920{,}000$); the smoothing length of $h = 0.125$ m is used for all numerical solutions. The figure shows that the reference solution only changes slightly when the particle spacing decreases.

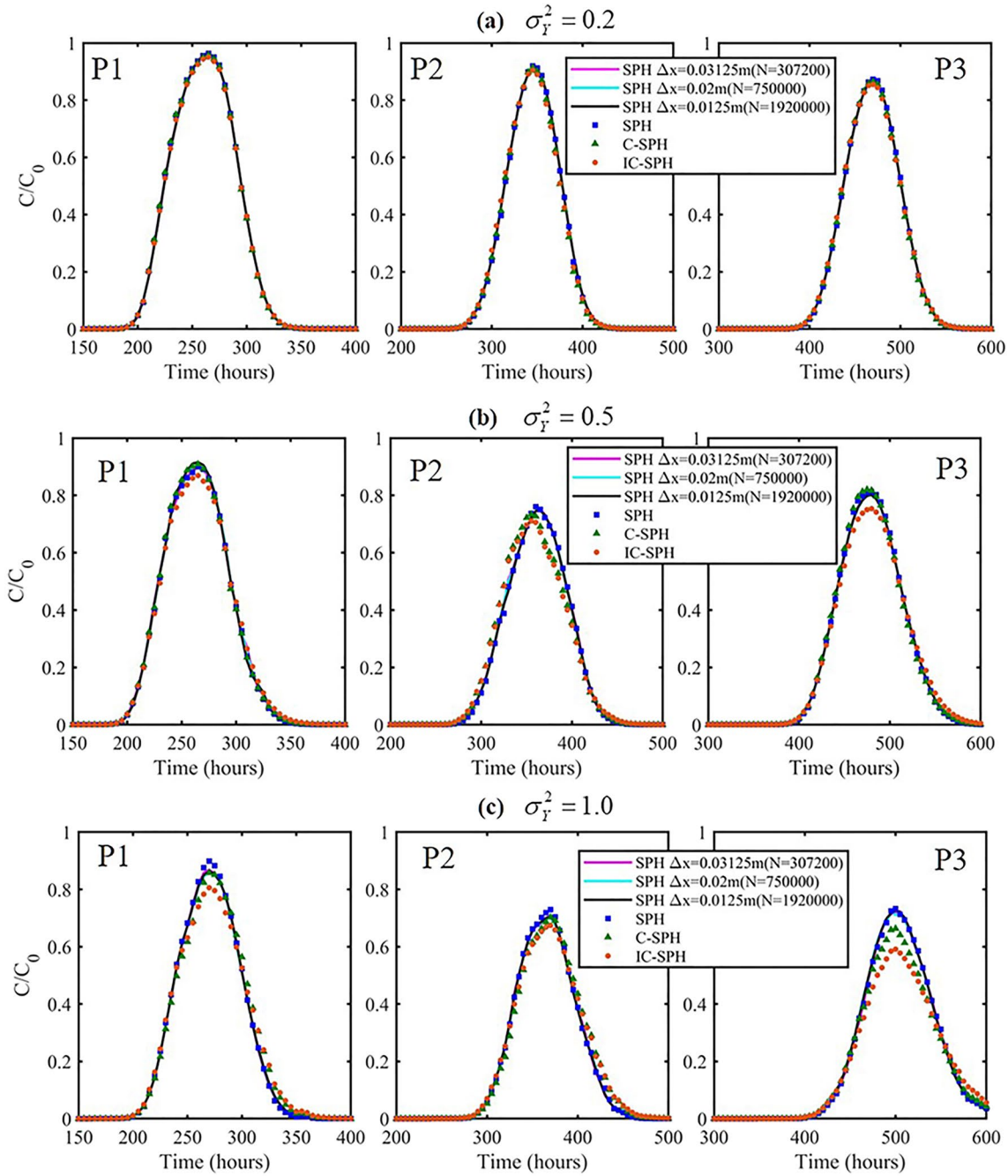

Figure B1. Breakthrough curves of normalized concentration (C/C_0) at points P1, P2, and P3 shown in Figure 5 for heterogeneous fields of hydraulic conductivity generated with (a) $\sigma_Y^2 = 0.2$, (b) $\sigma_Y^2 = 0.5$, and (c) $\sigma_Y^2 = 1.0$. The resolution for the finer Smoothed Particle Hydrodynamics (SPH) is $\Delta x = 0.03125$, 0.02, and 0.0125 m with smoothing length of $h = 0.125$ m.

When increasing the total number (N) of particles, it is always necessary to use a dynamical scheme to add more particles in the pathline-diverging areas or to use a particle shifting technology to obtain regularly distributed particles (Herrera et al., 2009; Zhang et al., 2019). These methods, however, are difficult to implement and computationally expensive.

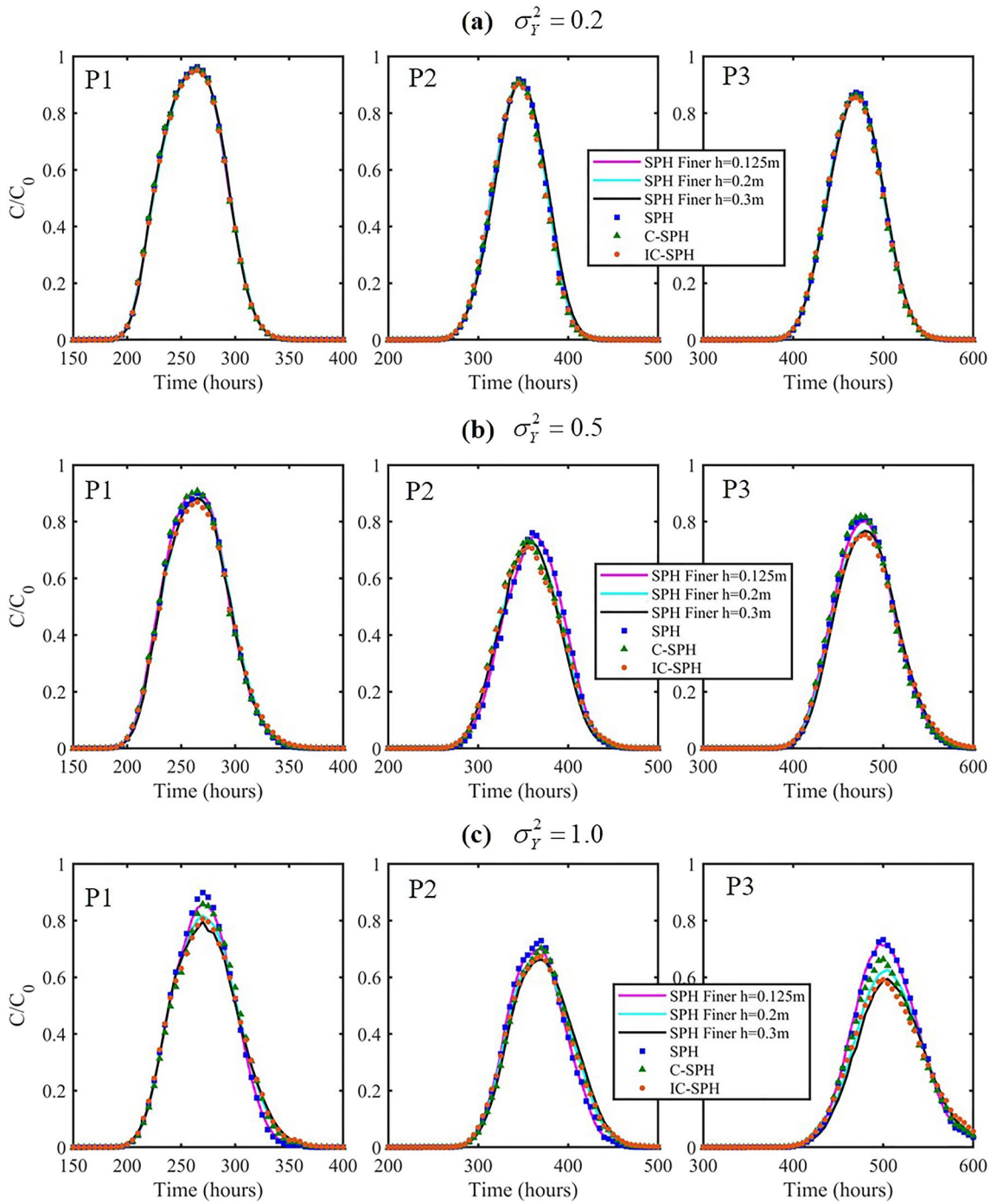

Figure B2. Breakthrough curves of normalized concentration (C/C_0) at points P1, P2, and P3 shown in Figure 5 for heterogeneous fields of hydraulic conductivity generated with (a) $\sigma_Y^2 = 0.2$, (b) $\sigma_Y^2 = 0.5$, and (c) $\sigma_Y^2 = 1.0$. The resolution for the finer Smoothed Particle Hydrodynamics (SPH) is $\Delta x = 0.02$ m with smoothing length of $h = 0.125$ m, 0.2 m, and 0.3 m.

Increasing the number of neighbor particles within a support domain can be achieved by increasing smoothing length h. This is illustrated in Figure B2 that plots the reference solutions with the same particle spacing of $\Delta x = 0.02$ m but with three different smoothing lengths of $h = 0.125$ m, 0.2 m, and 0.3 m. The smoothing length has a noticeable effect on the reference solutions. When h is increased from 0.125 to 0.3 m, the maximum concentration on the breakthrough curves decreases, as shown in Figure B2. This is also observed in Figure S4 in Supporting Information S1, indicating that the numerical discretizing error is dominant over the smoothing error and that using a larger smoothing length h reduces the numerical discretizing error. In other words, increasing h reduces the total error, although the smoothing error increases. When larger h is used, the reduced discretizing error is large than the increased smoothing error. Based on these analyses, we finally chose $\Delta x = 0.02$ m and $h = 0.3$ m for obtaining the reference solution based on SPH.

Data Availability Statement

The data and codes for reproducing the results of this study are available online at figshare via https://figshare.com/articles/dataset/Jiao_et_al_WRR_2021_zip/15131751 with DOI: 10.6084/m9.figshare.15131751.v1.

Acknowledgments
This study was supported by the National Natural Science Foundation of China (41877192). The first author was supported by the Fundamental Research Funds for National Universities to the China University of Geosciences (Wuhan) for her research at the Florida State University. The second author was supported by NSF Grant EAR-1552329.

References

Alvarado-Rodríguez, C. E., Sigalotti, L. D. G., & Klapp, J. (2019). Anisotropic dispersion with a consistent smoothed particle hydrodynamics scheme. *Advances in Water Resources*, *131*, 103374. https://doi.org/10.1016/j.advwatres.2019.07.004

Avesani, D., Dumbser, M., Vacondio, R., & Righetti, M. (2021). An alternative SPH formulation: ADER-WENO-SPH. *Computer Methods in Applied Mechanics and Engineering*, *382*, 113871. https://doi.org/10.1016/j.cma.2021.113871

Avesani, D., Herrera, P., Chiogna, G., Bellin, A., & Dumbser, M. (2015). Smooth particle hydrodynamics with nonlinear moving-least-squares WENO reconstruction to model anisotropic dispersion in porous media. *Advances in Water Resources*, *80*, 43–59. https://doi.org/10.1016/j.advwatres.2015.03.007

Batra, R. C., & Zhang, G. M. (2004). Analysis of adiabatic shear bands in elasto-thermo-viscoplastic materials by modified smoothed-particle hydrodynamics (MSPH) method. *Journal of Computational Physics*, *201*(1), 172–190. https://doi.org/10.1016/j.jcp.2004.05.007

Bear, J. (1972). *Dynamics of fluids in porous materials*. American Elsevier.

Beaudoin, A., Huberson, S., & Rivoalen, E. (2003). Simulation of anisotropic diffusion by means of a diffusion velocity method. *Journal of Computational Physics*, *186*(1), 122–135. https://doi.org/10.1016/s0021-9991(03)00024-x.s

Bellin, A., Rinaldo, A., Bosma, W. J. P., van der Zee, S. E. A. T. M., & Rubin, Y. (1993). Linear equilibrium adsorbing solute transport in physically and chemically heterogeneous porous formations 1. Analytical solutions. *Water Resources Research*, *29*(12), 4019–4030. https://doi.org/10.1029/93WR02303

Benson, D. A., & Meerschaert, M. M. (2008). Simulation of chemical reaction via particle tracking: Diffusion-limited versus thermodynamic rate-limited regimes. *Water Resources Research*, *44*, W12201. https://doi.org/10.1029/2008WR007111

Benson, D. A., Tomás, A., Diogo, B., Engdahl, N., Henri, C. V., & Fernàndez-Garcia, D. (2017). A comparison of Eulerian and Lagrangian transport and non-linear reaction algorithms. *Advances in Water Resources*, *99*, 15–37. https://doi.org/10.1016/j.advwatres.2016.11.003

Bolster, D., Paster, A., & Benson, D. A. (2016). A particle number conserving Lagrangian method for mixing-driven reactive transport. *Water Resources Research*, *52*, 1518–1527. https://doi.org/10.1002/2015WR018310

Boso, F., Bellin, A., & Dumbser, M. (2013). Numerical simulations of solute transport in highly heterogeneous formations: A comparison of alternative numerical schemes. *Advances in Water Resources*, *52*, 178–189. https://doi.org/10.1016/j.advwatres.2012.08.006

Chen, J. K., & Beraum, J. E. (2000). A generalized smoothed particle hydrodynamics method for nonlinear dynamic problems. *Computer Methods in Applied Mechanics and Engineering*, *190*(1–2), 225–239. https://doi.org/10.1016/S0045-7825(99)00422-3

Chen, J. K., Beraun, J. E., & Carney, T. C. (1999). A corrective smoothed particle method for boundary value problems in heat conduction. *International Journal for Numerical Methods in Engineering*, *46*, 231–252. https://doi.org/10.1002/(SICI)1097-0207(19990920)46:2<231::AID-NME672>3.0.CO;2-K

Clain, S., Diot, S., & Loubère, R. (2011). A high-order finite volume method for systems of conservation laws—Multi-dimensional optimal order detection (MOOD). *Journal of Computational Physics*, *230*, 4028–4050. https://doi.org/10.1016/j.jcp.2011.02.026

Cleary, P. W., & Monaghan, J. J. (1999). Conduction modelling using smoothed particle hydrodynamics. *Journal of Computational Physics*, *148*(1), 227–264. https://doi.org/10.1006/jcph.1998.6118

de Barros, F. P. J., Fiori, A., Boso, F., & Bellin, A. (2015). A theoretical framework for modeling dilution enhancement of non-reactive solutes in heterogeneous porous media. *Journal of Contaminant Hydrology*, *175–176*, 72–83. https://doi.org/10.1016/j.jconhyd.2015.01.004

Espanol, P., & Revenga, M. (2003). Smoothed dissipative particle dynamics. *Physical Review E*, *67*, 026705. https://doi.org/10.1103/PhysRevE.67.026705

Harbaugh, A. (2000). *MODFLOW-2000, the US Geological Survey modular groundwater model: User guide to modularization concepts and the ground-water flow process*. US Geological Survey.

Herrera, P. A., & Beckie, R. D. (2013). An assessment of particle methods for approximating anisotropic dispersion. *International Journal for Numerical Methods in Fluids*, *71*(5), 634–651. https://doi.org/10.1002/fld.3676

Herrera, P. A., Cortínez, J. M., & Valocchi, A. J. (2017). Lagrangian scheme to model subgrid-scale mixing and spreading in heterogeneous porous media. *Water Resources Research*, *53*, 3302–3318. https://doi.org/10.1002/2016WR019994

Herrera, P. A., Massabó, M., & Beckie, R. D. (2009). A meshless method to simulate solute transport in heterogeneous porous media. *Advances in Water Resources*, *32*(3), 413–429. https://doi.org/10.1016/j.advwatres.2008.12.005

Jubelgas, M., Springel, V., & Dolag, K. (2004). Thermal conduction in cosmological SPH simulations. *Monthly Notices of the Royal Astronomical Society*, *351*, 423–435. https://doi.org/10.1111/j.1365-2966.2004.07801.x

Konikow, L. F. (2011). The secret to successful solute-transport modeling. *Groudwater*, *49*(2), 144–159. https://doi.org/10.1111/j.1745-6584.2010.00764.x

Liu, G. R., & Liu, M. B. (2003). *Smoothed particle hydrodynamics: A meshfree particle method*. Singapore: World Scientific. https://doi.org/10.1142/5340

Liu, M. B., & Liu, G. R. (2006). Restoring particle consistency in smoothed particle hydrodynamics. *Applied Numerical Mathematics*, *56*(1), 19–36. https://doi.org/10.1016/j.apnum.2005.02.012

Liu, M. B., & Liu, G. R. (2010). Smoothed particle hydrodynamics (SPH): An overview and recent developments. *Archives of Computational Methods in Engineering*, *17*(1), 25–76. https://doi.org/10.1007/s11831-010-9040-7

Liu, M. B., Xie, W. P., & Liu, G. R. (2005). Modeling incompressible flows using a finite particle method. *Applied Mathematical Modelling*, *29*(12), 1252–1270. https://doi.org/10.1016/j.apm.2005.05.003

Monaghan, J. J. (2005). Smoothed particle hydrodynamics. *Reports on Progress in Physics*, *68*(8), 1703–1759. https://doi.org/10.1088/0034-4885/68/8/r01

Morris, J. P., Fox, P. J., & Zhu, Y. (1997). Modeling low Reynolds number incompressible flows using SPH. *Journal of Computational Physics*, *136*, 214–226. https://doi.org/10.1006/jcph.1997.5776

Nogueira, X., Ramírez, L., Clain, S., Loubère, R., Cueto-Felgueroso, L., & Colominas, I. (2016). High-accurate SPH method with multidimensional optimal order detection limiting. *Computer Methods in Applied Mechanics and Engineering*, *310*, 134–155. https://doi.org/10.1016/j.cma.2016.06.032

Pebesma, E. J. (2004). Multivariable geostatistics in S: The gstat package. *Computers & Geosciences*, *30*(7), 683–691. https://doi.org/10.1016/j.cageo.2004.03.012

Ren, J., Ouyang, J., & Jiang, T. (2015). An improved particle method for simulation of the non-isothermal viscoelastic fluid mold filling process. *International Journal of Heat and Mass Transfer*, *85*, 543–560. https://doi.org/10.1016/j.ijheatmasstransfer.2015.01.139

Ren, J., Ouyang, J., Jiang, T., & Li, Q. (2011). Simulation of complex filling process based on the generalized Newtonian fluid model using a corrected SPH scheme. *Computational Mechanics*, *49*(5), 643–665. https://doi.org/10.1007/s00466-011-0669-3

Sigalotti, L. D. G., Klapp, J., Rendón, O., Vargas, C. A., & Peña-Polo, F. (2016). On the kernel and particle consistency in smoothed particle hydrodynamics. *Applied Numerical Mathematics*, *108*, 242–255. https://doi.org/10.1016/j.apnum.2016.05.007

Sole-Mari, G., & Fernàndez-Garcia, D. (2018). Lagrangian modeling of reactive transport in heterogeneous porous media with an automatic locally adaptive particle support volume. *Water Resources Research*, *54*, 8309–8331. https://doi.org/10.1029/2018WR023033

Sole-Mari, G., Fernàndez-Garcia, D., Rodriguez-Escales, P., & Xavier Sanchez-Vila, X. (2017). A KDE-based random walk method for modeling reactive transport with complex kinetics in porous media. *Water Resources Research*, *53*, 9019–9039. https://doi.org/10.1002/2017WR021064

Sole-Mari, G., Schmidt, M. J., Pankavich, S. D., & Benson, D. A. (2019). Numerical equivalence between SPH and probabilistic mass transfer methods for Lagrangian simulation of dispersion. *Advances in Water Resources*, *126*, 108–115. https://doi.org/10.1016/j.advwatres.2019.02.009

Tartakovsky, A. M. (2010). Lagrangian simulations of unstable gravity-driven flow of fluids with variable density in randomly heterogeneous porous media. *Stochastic Environmental Research and Risk Assessment*, *24*(7), 993–1002. https://doi.org/10.1007/s00477-010-0402-3

Tartakovsky, A. M., & Meakin, P. (2005). A smoothed particle hydrodynamics model for miscible flow in three-dimensional fractures and the two-dimensional Rayleigh-Taylor instability. *Journal of Computational Physics*, *207*(2), 610–624. https://doi.org/10.1016/j.jcp.2005.02.001

Tartakovsky, A. M., Meakin, P., Scheibe, T. D., & Eichler West, R. M. (2007a). Simulations of reactive transport and precipitation with smoothed particle hydrodynamics. *Journal of Computational Physics*, *222*(2), 654–672. https://doi.org/10.1016/j.jcp.2006.08.013

Tartakovsky, A. M., Meakin, P., Scheibe, T. D., & Wood, B. D. (2007b). A smoothed particle hydrodynamics model for reactive transport and mineral precipitation in porous and fractured porous media. *Water Resources Research*, *43*, W05437. https://doi.org/10.1029/2005WR004770

Tartakovsky, A. M., Tartakovsky, G. D., & Scheibe, T. D. (2009). Effects of incomplete mixing on multicomponent reactive transport. *Advances in Water Resources*, *32*(11), 1674–1679. https://doi.org/10.1016/j.advwatres.2009.08.012

Tartakovsky, A. M., Trask, N., Pan, K., Jones, B., Pan, W., & Williams, J. R. (2015). Smoothed particle hydrodynamics and its applications for multiphase flow and reactive transport in porous media. *Computational Geosciences*, *20*(4), 807–834. https://doi.org/10.1007/s10596-015-9468-9

Xu, X., & Deng, X. L. (2016). An improved weakly compressible SPH method for simulating free surface flows of viscous and viscoelastic fluids. *Computer Physics Communications*, *201*, 43–62. https://doi.org/10.1016/j.cpc.2015.12.016

Yildiz, M., Rook, R. A., & Suleman, A. (2009). SPH with multiple boundary tangent method. *International Journal for Numerical Methods in Engineering*, *77*(10), 1416–1438. https://doi.org/10.1002/nme.2458

Zhang, G. M., & Batra, R. C. (2004). Modified smoothed particle hydrodynamics method and its application to transient problems. *Computational Mechanics*, *34*(2), 137–146. https://doi.org/10.1007/s00466-004-0561-5

Zhang, G. M., & Batra, R. C. (2008). Symmetric smoothed particle hydrodynamics (SSPH) method and its application to elastic problems. *Computational Mechanics*, *43*(3), 321–340. https://doi.org/10.1007/s00466-008-0308-9

Zhang, Z. L., & Liu, M. B. (2018). A decoupled finite particle method for modeling incompressible flows with free surfaces. *Applied Mathematical Modelling*, *60*, 606–633. https://doi.org/10.1016/j.apm.2018.03.043

Zhang, Z. L., Walayat, K., Huang, C., Chang, J. Z., & Liu, M. B. (2019). A finite particle method with particle shifting technique for modeling particulate flows with thermal convection. *International Journal of Heat and Mass Transfer*, *128*, 1245–1262. https://doi.org/10.1016/j.ijheatmasstransfer.2018.09.074

Zhu, G. X., Zou, L., Chen, Z., Wang, A. M., & Liu, M. B. (2018). An improved SPH model for multiphase flows with large density ratios. *International Journal for Numerical Methods in Fluids*, *86*(2), 167–184. https://doi.org/10.1002/fld.4412

Zhu, Q., Hernquist, L., & Li, Y. (2015). Numerical convergence in smoothed particle hydrodynamics. *The Astrophysical Journal*, *800*, 6. https://doi.org/10.1088/0004-637x/800/1/6

Zimmermann, S., Koumoutsakos, P., & Kinzelbach, W. (2001). Simulation of pollutant transport using a particles method. *Journal of Computational Physics*, *173*(1), 322–347. https://doi.org/10.1006/jcph.2001.6879